Sandstone body character, river styles, and geomorphology of the lower Eocene Willwood Formation, Bighorn Basin, Wyoming, USA

Youwei Wang[1 *], Timothy F. Baars[1], Hiranya Sahoo[1], Joep E.A. Storms[1], Allard W. Martinius[1,2], Philip Gingerich[3], Hemmo A. Abels[1]

[1] Department of Geosciences and Engineering, Delft University of Technology, Stevinweg 1, 2628 CN Delft, the Netherlands

[2] Equinor ASA, Arkitekt Ebbellsvei 10, N–7053 Trondheim, Norway

[3] Museum of Palaeontology, University of Michigan, Ann Arbor, MI 48109-1079, USA

*Correspondence email: y.wang.delft@outlook.com

Abstract:

The lower Eocene Willwood Formation of the intermontane Bighorn Basin, Wyoming, USA, is an alluvial red bed succession with a sand content of ca. 20%-25%. The formation has been studied intensively for paleontology, paleoclimate, and sedimentary reconstruction. However, alluvial sandstone bodies and their corresponding river styles remain little characterized and documented. Here, efforts are made to study the characteristics and river styles of sandstone bodies through ca. 300 m of alluvial stratigraphy in the McCullough Peaks outcrop area based on the field data and a georeferenced 3-D photogrammetric model. Four channel facies associations are recognized, and they are ascribed to four river planform styles: distributary channel, massive trunk-shaped channel, braided channel, and sinuous channel, with the latter two styles being the more abundant. The channel sandstone bodies that show the character of sinuous rivers and those of braided rivers differ significantly in average thickness (6.1 m versus 9.0 m) and insignificantly in average width (on average 231 m) and paleoflow directions (on average N003). Braided-character dominated and sinuous-character dominated river styles are seen to alternate in the outcrop, while they show no spatial dependency in the 10 km^2 study area. Bighorn Basin margins varied in the early Eocene,

with differing tectonic, geological, and topographic characteristics. The observed mixture of river styles may be attributed to differential influences of axial and transverse river systems and/or climate change that controls water discharge and sediment load. An early Eocene geomorphologic reconstruction is constructed summarizing these new and earlier results.

Keywords: Bighorn Basin, Willwood Formation, channel sandstone body, river style

1. Introduction

Alluvial architecture illustrates the size, shape, and spatial arrangement of fluvial channel bodies and their associated facies in three dimensions (Allen, 1978; Bridge & Leeder, 1979). The architecture is controlled by both autogenic processes, such as channel avulsion and self-organization (e.g. Mackey & Bridge, 1995; Hajek *et al.*, 2010), and allogenic factors, such as eustasy, climate, and tectonics (e.g. Shanley & McCabe, 1994; Holbrook *et al.*, 2006; Hampson *et al.*, 2013; Bijkerk *et al.*, 2014). Extensive studies have been conducted on alluvial deposits using various approaches and datasets, including high-resolution three-dimensional seismic data (e.g. Posamentier *et al.*, 2007), numerical modeling (e.g. Jerolmack & Paola, 2007; Karssenberg & Bridge, 2008; Wang *et al.*, 2021a), and outcrop analogs (e.g. Allen *et al.*, 2013; Colombera *et al.*, 2016, 2017; Ghinassi *et al.*, 2016; Ghinassi & Ielpi, 2018). Outcrop analogs provide data that span large hierarchical temporal and spatial scales, which can help interpret depositional environments, reconstruct palaeoclimates (e.g. Howell *et al.*, 2014; Colombera *et al.*, 2016; Paredes *et al.*, 2016), and build subsurface predictive models (e.g. Bryant *et al.*, 2000; Enge *et al.*, 2007).

By utilizing alluvial strata in the Bighorn Basin, numerous studies have investigated a variety of aspects: e.g., paleontology (Gingerich, 2010); palaeo-magnetism (Clyde *et al.*, 1994); and, especially, palaeosols (Kraus & Gwinn, 1997; Kraus, 1999, 2002; Abels *et al.*, 2013; Wang *et al.*, 2021b). In contrast, the alluvial sandstone body character and spatial distribution are less well documented and analyzed. The well-documented floodplain cyclicity in the Willwood Formation of the Bighorn Basin provides an opportunity to investigate the influence of orbital climate forcing on alluvial architecture (Abdul Aziz *et al.*, 2008; Abels *et al.*, 2013). Also, extreme climate warming has been observed to impact alluvial architecture in the basin (Foreman, 2014; Van der Meulen *et al.*, 2020). Generic relationships between channel and floodplain deposits were illustrated over basin scales, with thick sheet sandstones ascribed to results of meandering river processes (Kraus & Gwinn, 1997). Coarse-grained and conglomeritic braided channel deposits were described in the west of the basin (Neasham & Vondra, 1972; Kraus, 1985). Detailed sedimentological description was conducted by Foreman (2014) on the PETM boundary sandstones. Owen *et al.* (2017, 2019) performed a basin-scale classification of fluvial architecture, with their work and the others providing a basin-scale context for this study.

Here, efforts are made to characterize channel sandstone bodies in terms of geometry and internal characteristics, reconstruct their related river styles, and fit them in the basin-scale geomorphology. An integrated field analysis is performed on the alluvial sandstone bodies in the McCullough Peaks area of the Bighorn Basin (Figure 1), combining field documentation with observations in a georeferenced photogrammetric model developed using an unmanned aerial vehicle (UAV). The objectives of this study are fourfold: (1) to document lithofacies and lithofacies associations, (2) to attribute lithofacies associations to most possible corresponding river styles, (3) to analyze the distributions of the river styles over space, and (4) to reconstruct the early Eocene geomorphology of the Bighorn Basin.

2. Geological background

2.1 Structural setting

The Bighorn Basin is a Laramide intermontane basin with a length of ~200 km and a width of ~80 km. It was bounded by the western Beartooth Mountains, southwestern Washakie Range, eastern Bighorn Mountains, and the northeastern Pryor Mountains during Paleocene to Early Eocene (Foose *et al.*, 1961; Lillegraven & Ostresh, 1988). Drainage of the basin was toward the north and northeast during deposition of the Willwood Formation. The Absaroka Range was formed by volcanic activity during the late early and middle Eocene (Smedes and Prostka, 1972), which makes it challenging to constrain the southwestern margin of the Bighorn Basin in the Eocene. The eastern margin of the basin has always been a relatively gentle slope (Yonkee & Weil, 2015).

2.2 Palaeoclimate

The global early Eocene is indicated to be in a hothouse state, with a globally average temperature ~12°C higher than the present global average (Westerhold *et al.*, 2020; Scotese *et al.*, 2021). The early Eocene Bighorn Basin is suggested to have been in a warm-temperate to a subtropical environment with seasonal precipitation (Van Houten, 1948). The basin landscape is suggested to resemble modern-day savannahs, with broad open areas interspersed with forest-bordering streams (Neasham, 1967). Two hyperthermal events are recorded in the upper part of the study interval, referred to as H1/ETM2 and H2 (Abels *et al.*, 2016; Figure 1).

2.3 Depositional setting

The Willwood Formation consists of a series of lower Eocene alluvial deposits that are currently exposed in the central part of the basin roughly along the NNW-SSE-extending basin axis (Figure 1). It is mainly composed of sandstones, siltstones, and mudstones, parts of which have undergone intensive pedogenic modification (Kraus & Davies-Vollum, 2004). Extensive studies have been carried out, with main focus on palaeosols (Kraus, 1999, 2002), processes of river avulsion (Neasham & Vondra, 1972; Kraus & Gwinn, 1997; Kraus & Davies-Vollum, 2004), and fluvial cyclicity (Abdul Aziz *et al.*, 2008; Abels *et al.*, 2013). The dominant palaeoflow direction is interpreted to be NNW to NNE (Neasham & Vondra, 1972; Owen *et al.*, 2017, 2019). Cyclic palaeosol maturation patterns associated with heterolithic avulsion deposits have been inferred as the result of allogenic forcing (Kraus & Aslan, 1993; Abdul Aziz *et al.*, 2008; Abels *et al.*, 2013; Wang *et al.*, 2021b). The sediment accumulation rate has been estimated by various studies, showing a range of 288 to 391 m/Myr (Clyde *et al.*, 1994; Westerhold *et al.*, 2007; Stap *et al.*, 2009; Gingerich, 2010; Abels *et al.*, 2012, 2013; Wang *et al.*, 2021b).

2.4 Tectonics and possible provenances

Neasham and Vondra (1972) suggested most Willwood sandstone units to be subarkose, with a mainly western source. In contrast, Kraus & Middleton (1987) indicated that most sandstone bodies in their study area (the Clarks Fork Basin in front of the Beartooth Range) are litharenites, with the main source area in the Beartooth Mountains. Other work indicates the presence of multiple provenances, including all the mountainous areas expressed before or during the early Eocene (e.g. Owen *et al.*, 2019).

Beartooth Mountains to the northwest

The major uplift of the Beartooth Mountains took place during the mid-to-late Paleocene (Gingerich, 1983). The eastern flank of the Beartooth Mountains was very steep, with ca. 8000 m of structural relief (Wise, 2000). According to the work by DeCelles *et al.* (1991), the Beartooth fluvial systems are comprised of several ephemeral coarse-grained alluvial fans and braid-plain deposits. Lacustrine deposits are reported in the northwest of Powell, in the mountain front close to the Polecat Bench area (Figure 1; Yuretich *et al.*, 1984).

Absaroka Mountains to the west

The Absaroka Mountains forming the western margin of the present-day Bighorn Basin were not emplaced until near the end of Willwood Formation deposition, since volcanic activity started in the middle early to middle Eocene (Smedes & Prostka, 1972; Sundell, 1990). This makes it challenging to understand the original catchment of the Bighorn Basin fluvial system.

Washakie Range to the west

It is suggested that the Washakie Range, present during the Paleocene and early Eocene, was located farther west of the current western basin boundary, with a steep front towards the east (Kraus, 1983, 1985; Lillegraven, 2009). Overthrusting associated with the formation of the mountain range is likely to have influenced the development of the Willwood sedimentary sequences (Yonkee & Weil, 2015), thus making it difficult to constrain the characteristics of the fluvial system fed by this source terrain. According to Owen *et al.* (2019), at the time the Willwood system was active, it was characterized as a distributive fluvial system, with conglomeratic input from the Washakie Range. Kraus (1984) reported early Eocene fanglomerates in the alluvial fan system sourcing from this range.

Owl Creek Mountains to the south

The uplift around the southern margin of the basin formed the southern Bighorn and Owl Creek Mountains, which were subsequently thrust southward in the early-mid Eocene. In general, the northern slope of Owl Creek Mountains was gentle (not steeply faulted) during the early Eocene, and the southern part of the Bighorn Basin was relatively low, probably only forming a gentle rise separating the Bighorn Basin from the Powder River Basin in the south (Wing & Bown, 1985).

Bighorn Mountains to the southeast and east

The Bighorn Mountains have a long shallowly dipping slope on the Bighorn Basin side and a steep thrust scarp on the Powder River Basin side (Yonkee & Weil, 2015). Swampy and lacustrine deposits are indicated to be present in front of the Bighorn Mountains on the Bighorn Basin side (Wing & Bown, 1985; Davies-Vollum & Wing, 1998). There might be large fluvial systems along the western side of the Bighorn Mountains, but they may contribute less and finer sediment to the McCullough Peaks study area given the shallow gradient and consequently less energy there. Westerly palaeocurrents are rarely documented in the eastern and southeastern parts of the basin (Owen *et al.*, 2019), suggesting that the eastern side of the basin might have contributed little to the basinal fluvial system.

Pryor Mountains to the northeast

The Pryor Mountains are interpreted to be asymmetric anticlines that experienced overthrusting in the later stages (Blackstone, 1940). Their contribution as a significant catchment is not supported by the palaeocurrent data (Seeland, 1998). There was a "Pryor Gap" between the Pryor Mountains and the Bighorn Mountains (see Figure 2 in Blackstone, 1940), which could have served as a possible exit for the fluvial system during the deposition of the Willwood Formation.

3. Dataset and methodology

3.1 Fieldsite documentation

Sandstone bodies were systematically documented in the field (Figure 2) using a standard set of parameters including grain size, lithology, sedimentary structure, geometry, boundaries, palaeo-flow directions, and dimensions. Based on these documentations, lithofacies and lithofacies association classification schemes are established following methods outlined by Miall (1985, 1996) and Allen (1983). Data were collected in comprehensive spreadsheets and short sedimentary logs to characterize each sandstone body type. The grain size was measured by observing the grains together with a grain size chart under a hand lens. Dimensions of sandstone bodies were measured using Jacob's staff, flexible tapes, and a laser rangefinder when not directly accessible. The color was described according to the methods detailed in the Soil Survey Manual (Soil Survey Division Staff, 1993). Palaeocurrent data and cross-set thickness were measured from dune-scale cross-stratification (mainly planar and trough cross-stratification).

3.2 UAV-based photogrammetry

The preparation of the UAV-based photogrammetric model has been detailed in Wang *et al.* (2021b). The model includes 21144 photos taken on 34 flights and it covers a total area of ~10 km^2, with approximate north-south and east-west lengths of 2.5 km and 4 km, respectively. The studied stratigraphic succession is ~300 m thick and dips at ~2° towards the south. Fifty-seven ground control points (GCPs) were placed, contributing to centimeter accuracy relative to the local base station. Agisoft PhotoScan (Version 1.4.3, July 2018; current Metashape) was used to build the 3-D digital models, which were later imported into LIME (version 2.2.2; Buckley *et al.*, 2019) for visualization and interpretation.

3.3 Petrological analysis

A total of 32 sandstone samples were collected from outcrops in the study area and made into thin sections in the laboratory. Classification of sandstones follows the scheme by Mcbride (1963) that groups framework grains into (1) quartz plus chert and quartzite, (2) feldspar, and (3) rock fragments and accessory minerals.

3.4 Formative bankfull depth estimation

Dune-scale cross-set thickness (S_m) has been empirically used to estimate the mean formative bedform height (h_m), as is shown in Eq. 1 (Bridge & Tye, 2000; Leclair & Bridge, 2001). The application of this method requires to meet the precondition that the coefficient of variation (ratio of standard deviation to mean) of the preserved cross-set thickness should vary between 0.58 and 1.18 (Bridge & Tye, 2000).

$$h_m = 2.9\ (\pm 0.7)\ S_m \tag{1}$$

Then, the mean formative bankfull depth (d) can be estimated based on the empirical equation proposed by Bradley & Venditti (2017):

$$d = 6.7\ h_m \text{ (with 50\% prediction interval: } 4.4\ h_m \text{ to } 10.1\ h_m) \tag{2}$$

3.5 Statistical analysis

Two-sample t-tests are performed to assess whether the differences between parameters of different types of deposits are statistically significant. Paleocurrent data are analyzed as circular data using the R programming language, and the Rayleigh Test of Uniformity is implemented to check whether the distribution is significantly different from the uniform distribution. Watson’s Two-Sample Test of Homogeneity is employed to compare whether the two distributions are significantly different from each other.

4. Results

4.1 Lithofacies analysis

Based on detailed observation and description of grain size, lithology, internal sedimentary structures, and spatial positions in the sandstone bodies, a total of 12 lithofacies are recognized in the field (Figure 3 and Table 1). There is one conglomeratic lithofacies, named clast-supported conglomerate (G);

there are nine sandy lithofacies, including massive sandstone (Sm), trough cross-stratified sandstone (St), planar/tabular cross-stratified sandstone (Sp), ripple cross-laminated sandstone (Sr), climbing-ripple cross-laminated sandstone (Scr), low-angle (<15°) cross-stratified sandstone (Sl), sandstone with erosional scour and fill (Se), bioturbated sandstone (Sb), and convoluted sandstone (Sc); there are two silty to muddy lithofacies: mudstones and siltstones (Fs) and laminated siltstones (Fl). Details of their character and interpretation are given in Table 1.

4.2 Facies association analysis

According to the organizations of lithofacies in the vertical succession and lateral distribution (Table S1), a total of 6 facies associations are classified, which fall into two major categories, namely channel facies associations and floodplain facies associations. They are described and interpreted in the following sections, though petrological and statistical analyses are not done in all facies associations.

4.2.1 Channel facies associations

(1) Facies Association 1: small-scale cut-and-fill channel sandstone deposits

Description:

Facies Association 1 (FA1) is mainly comprised of fine- to medium-grained sandstone bodies, with a thickness range of 0.5-3 m. Its indurated part shows a lenticular external geometry with concave-up margins in the transverse view (Figure 4A) and ribbon-shaped geometry in the longitudinal view (Figure 4B). Various lithofacies are present, including trough cross-stratified sandstone (St), planar/tabular cross-stratified sandstone (Sp), and ripple cross-laminated sandstone (Sr). Within FA1, trough cross-stratified sandstone (St), if present, is usually in the lower part, planar/tabular cross-stratified sandstone (Sp) in the middle part, and ripple cross-laminated sandstone (Sr) in the upper part. This facies association is generally encased within floodplain deposits that present pedogenic features due to subaerial exposure. The contact between FA1 and floodplain fines is usually sharp with floodplain fines passively draping the top of the sandstone body. A total of 15 FA1 sandstone bodies are documented in the field.

Interpretation:

FA1 is interpreted to be the product of relatively straight crevasse channels/floodplain distributaries (cf. Kraus & Gwinn, 1997; Clyde & Christensen, 2003; Gibling, 2006), also known as feeder channels of the avulsion complex (cf. Davies-Vollum & Kraus, 2001). The sharp contact with floodplain fines indicates an erosional base, the massive structure indicates rapid cut-and-fill processes, and the presence of cross-bedding suggests downstream traction of stream power. Similarly, at localities in the vicinity of the study area, this type of sandstone bodies is reported to be generally thinner than 3 m (Kraus, 1997; Clyde & Christensen, 2003) and referred to as ribbon sandstone bodies (Kraus & Middleton, 1987).

(2) Facies Association 2: large-scale, massive, trunk-shaped channel sandstone deposits

Description:

Facies Association 2 (FA2) is mainly composed of fine- to medium-grained sandstone (Figure 5), with a thickness of commonly >8 m. FA2 deposits generally present channelized features with clear gradually-thinning channel wings (Figure 5A). There is usually an erosional channel base formed by trough cross-stratified sandstone (St), above which trough cross-stratified sandstone (St), planar/tabular cross-stratified sandstone (Sp), and ripple cross-laminated sandstone (Sr) dominate, with occasionally seen convoluted sandstone (Sc; Figs. 5B and 5C). At some locations, FA2 appears to be present in massive sandstone bodies that are scant with internal erosional surfaces and abundant with sharp channel margins (Figure 5D). FA2 is relatively rare (5 out of 92 documented channel sandstone bodies) in the study area. Although not always, it mostly (3 out of 5 cases) occurs at the similar/same stratigraphic level as the sinuous channel sandstone deposits (FA4), which will be comprehended later.

Interpretation:

FA2 presents characteristics that are usually ascribed to the sedimentary product of large-scale river processes without obvious downstream and lateral accretion. Great sandstone body thickness (>8 m), steep channel margin (e.g. Figure 5E), and the erosional base of the sandstone body indicate deep and strong scouring behaviors. Nonetheless, its origin is still not well understood yet due to the scarcity of FA2 in the study area and thus lack of data.

(3) Facies Association 3: braided channel sandstone deposits

Description:

Facies Association 3 (FA3) is generally comprised of medium-grained sandstones, with conglomerate (G) occasionally seen at the base as lag deposits (Figure 6). It is usually multi-storied, with the thickness varying between 4 m and 8 m; a single-story unit within it is generally 0.5-2 m thick. Sharp erosional bases are present between stories. Within a single story, there are usually sandstone with erosional scour and fill (Se) and trough cross-stratified sandstone (St) in the lower part, planar/tabular cross-stratified sandstone (Sp) in the middle part, as well as ripple cross-laminated sandstone (Sr) and low-angle (<15°) cross-stratified sandstone (Sl) in the upper part, with occasionally seen massive sandstone (Sm; Figure 6D). The dip direction of the accretion surfaces is generally parallel to measured palaeocurrent directions in cross-bedded sets.

Forty-eight FA3 sandstone bodies are documented in this study, with an average thickness of 6.1 m and a standard deviation of 2.4 m (Figure 7A). Their apparent widths measured in the photogrammetric model were corrected using the average paleoflow direction (N004; Figure S1; Fabuel-Perez *et al.*, 2009), yielding an average of 203 m and a standard deviation of 137 m (Figure 7B). These braided channel sandstone bodies commonly have 3-4 stories, with an average story thickness of 1.7 m. The sandstone body aspect, defined as the width/thickness ratio, has an average of 38 and a standard deviation of 28 (Figure 7C). Dune-scale cross-sets in FA3 (n =45) have an average thickness of 22 cm, with a standard deviation of 13 cm and a coefficient of variation (CV) of 0.59 (Figure 7D). Using these dune-set data and employing existing empirical relationships (e.g., Bridge & Tye, 2000; Leclair & Bridge, 2001), the average bankfull depth is estimated to be 4.3 m (22 cm × 2.9 × 6.7). The high CV (0.59) ensures the reliability of the estimation of the formative flow depth using cross-set thickness (Bridge & Tye, 2000). Planar/tabular cross-stratified sandstone (Sp) and low-angle (<15°) cross-stratified sandstone (Sl) are dominant lithofacies in

FA3 when it comes to their proportions in thickness, accounting for 51% and 15%, respectively (Figure 7E). Palaeoflow rose diagram shows a mean flow direction of N016 and a standard deviation of 90° (Figure 7F). The distribution of the paleoflow data is significantly different from the uniform distribution according to the Rayleigh test of uniformity (0.29 with a p-value of 0).

Microscopic observation of 28 thin sections shows that monocrystalline quartzs in FA3 are generally subrounded to subangular and slightly spherical (Figure S2A and S2B), and they are classified together with polycrystalline quartz (quartzite), and microcrystalline quartz (chert) as "quartz" in the scheme developed by McBride (1963). Feldspar content widely varies, with potash feldspar (e.g. orthoclase and microcline) more dominant than plagioclase (e.g. albite). Rock fragments include sedimentary, volcanic, and metamorphic components. Accessory (heavy) minerals are either of igneous or metamorphic origin, and include magnetite, zircon, tourmaline, and hornblende. Both calcite and silica cement are observed, with the former one contributing to the mosaic granular framework, while the latter caused euhedral to subhedral quartz/feldspar overgrowths.

Interpretation:

FA3 presents the characteristics that are normally ascribed to the sedimentary product of braided river processes. This interpretation is supported by the predominance of medium to coarse-grained bedload material (Foreman, 2014), the scarcity of lateral accretion deposits, the abundance of downstream accretion deposits, and the stacking of several single-story units within individual sandstone bodies (Gibling, 2006). The presence of some fine-grained deposits below erosional surfaces suggests channel abandonment and reoccupation. Single-story units in FA3 are generally narrow and thin, indicating their short life-spans and quick lateral coalescence of multiple channel stories (Gibling, 2006). In general, braided channels are believed to result from high sediment load, coarse sediment grain size, high gradient, and weak overbank materials (Church, 2006; Schumm, 1985).

(4) Facies Association 4: sinuous channel sandstone deposits

Description:

Facies Association 4 (FA4) is generally composed of (1) poorly sorted, subangular, coarse-grained trough cross-stratified sandstones (St) with granules (G) and sandstones with erosional scour and fill (Se) at the base, (2) large-scale inclined strata with moderate to well-sorted medium-grained trough cross-stratified sandstones (St) and planar cross-stratified sandstones (Sp) in the middle, and (3) fine-grained ripple-laminated sandstones (Sr) at the top (Figure 8). The basal part is usually 0.5-1 m thick, while the middle and upper parts are generally >4 m thick. Both dune-scale cross-stratification (Figure 8D) and ripple-scale cross-lamination sedimentary structures are present. Accretion beds (Figure 8B) are inclined approximately perpendicular to or at a large angle with measured palaeocurrent directions. Water-escape structures are occasionally seen in convolute sandstone (Sc) within lateral accreted deposits (Figure 8C). The presence of one well-preserved extensive channel belt oriented in the downstream direction makes it possible to calculate its channel sinuosity index in the photogrammetric model (Figure S1H), which is 1.8 and thus falls in the meandering river category (Williams, 1986).

Thirty-nine sandstone bodies with FA3 are documented. The average thickness is 9.0 m while the standard deviation is 2.7 m (Figure 7A). Apparent field measurements of these sandbodies are corrected against the average paleoflow direction (N004; Figure S1), yielding an average value of 266 m and a standard deviation of 203 m (Figure 7B). The sandstone body aspect has an average of 31 and a standard deviation of 21 (Figure 7C). Dune-scale cross-sets in FA4 (n =11) have an average thickness of 26 cm with a standard deviation of 7 cm and thus a coefficient of variation (CV) of 0.29 (Figure 7D). From these data and the application of existing empirical relationships (Bridge and Tye, 2000; Leclair and Bridge, 2001), the average bankfull depth is calculated to be 5.1 m (26 cm × 2.9 × 6.7). The low CV (0.29, required to range between 0.58-1.18) renders it uncertain to estimate the formative flow depth using cross-set thickness (Bridge and Tye, 2000). Planar/tabular cross-stratified sandstone (Sp) and trough cross-stratified sandstone (St) are predominant lithofacies in terms of the lithofacies proportions in thickness, accounting for 45% and

23%, respectively (Figure 7E). The palaeoflow measurements (n = 63) present a mean flow direction of N332, with a standard deviation of 98° (Figure 7F). The distribution of the paleoflow data in FA4 is significantly different from the uniform distribution according to the Rayleigh test of uniformity (0.23 with a p-value of 0.04).

Compared with FA3 braided channel sandstone bodies, sinuous counterparts are significantly thicker ($t = 5.3$, $p = 0.9\times10^{-7}$) and insignificantly wider ($t = 1.4$, $p = 0.16$) according to the t-test. However, dune-scale cross-sets in FA4 sinuous channel deposits are not significantly different from those in FA3 braided channel deposits ($t = 0.6$, $p = 0.5$), although the average of the former is thicker than that of the latter. In terms of paleoflow measurements, there is no significant difference between braided and sinuous channel deposits at 0.05 level of significance according to Watson's Two-Sample Test of Homogeneity, which is likely attributable to the large standard deviations of both measurements (90° and 98°, respectively).

There are 3 available thin sections for FA4 sandstone. Compared with FA3, FA4 is overall finer and has higher abundances of quartz and chert (Figure S2C and S2D).

Interpretation:

FA4 presents the characteristics that are normally ascribed to the sedimentary product of sinuous river processes. Accretion beds are aligned broadly perpendicular to the overall paleoflow direction, and they are inferred as lateral accretion beds (Figure 8B). These lateral accreted deposits result from the reduced shear stress associated with helicoidal flows, which leads to erosion in the outer bend and lateral migration of the point bar located in the inner bend in the same direction (Bridge, 1993). The coarser-grained lower segment of the sandstone bodies represents the channel lag interval. In general, sinuous channels are believed to result from a perennial flow, a relatively low sediment load, a low gradient, and cohesive overbank materials (Church, 2006; Schumm, 1985).

4.2.2 Floodplain facies associations

The floodplain deposits have been extensively described in numerous studies (e.g. Kraus, 1987; Kraus & Bown, 1993; Kraus & Gwinn, 1997; Kraus & Hasiotis, 2006; Abdul Aziz *et al.*, 2008; Abels *et al.*, 2013; Wang *et al.*, 2021b), and thus only a comprehensive summary is provided here.

(1) Facies Association 5: crevasse splay deposits

Description:

Facies Association 5 (FA5) consists of very fine- to coarse-grained sandstones (Figure 9A). It is often composed of multiple beds, with the thickness of an individual bed ranging from 0.1 m to 0.5 m. FA5 sediments are in general well sorted. Trough cross-stratified sandstone (St), low-angle (<15°) cross-stratified sandstone (Sl), and ripple cross-laminated sandstone (Sr) are the most dominant lithofacies, typically presenting upward coarsening trends. The lateral extent of FA5 can be up to a few kilometers as measured from the photogrammetric model and traced in the field. Burrows are observed to be oriented in random directions (Sb in Figure 3). The palaeocurrents measured in FA5 deposits are generally oblique to the main channel from which the deposit originates. FA5 deposits are prevalent in the whole stratigraphy, forming the 'heteolithic' deposits of Abels *et al.* (2013).

Interpretation:

FA5 is interpreted to represent unconfined flow conditions on the floodplain, as part of a splay complex formed during erosion of the channel levee (Davies-Vollum & Kraus, 2001; Fisher *et al.*, 2007). Multiple beds may represent multiple events of crevasse processes. FA5 has been commonly referred to as heterolithic deposits produced by avulsion processes (*e.g.* Kraus & Aslan, 1993, Kraus & Wells, 1999, Abels *et al.*, 2013).

(2) Facies Association 6: overbank palaeosol deposits

Description:

Facies Association 6 (FA6) is the most dominant facies association in the study area (Figs. 9B and 9C), and it is mainly comprised of claystones, mudstones, and sandy siltstones, with coarser materials (sandy siltstones) in the lower parts and finer materials (claystones and mudstones) in the upper part (Abels *et al.*, 2013). Various matrix colors are seen including light grey, black, (dark) reddish-brown, purple, olive, and bright yellowish-brown. The color of the same palaeosol layer is found to be stronger in the place where sandstone bodies underlie. There are broadly two types of FA6 deposits in terms of pedogenic strength, namely moderately pedogenically modified ones and strongly pedogenically modified ones, the latter of which is featured by abundant mottling and nodules (Retallack, 2001). Similarly, Abels *et al.* (2013) proposed to divide FA6 deposits into three main types according to the colors, including purple, purple-red, and red types, which differ in various aspects, such as the commonly observed carbonate nodules in purple-red and red FA6 deposits and contrastingly absent carbonate nodules in purple FA6 deposits. More details including cyclic features of palaeosols in the study area have been provided and comprehensively analyzed by Abels *et al.* (2013) and Wang *et al.* (2021b).

Interpretation:

FA6 is interpreted to result from overbank deposition (Bown & Kraus, 1987; Abels *et al.*, 2013). The extensive presence of intersecting slickensides suggests that FA6 is mainly the result of vertic palaeosol formation (Soil Survey Division Staff, 1993; Abels *et al.*, 2013). Different drainage conditions are inferred according to the carbonate content and colors of various palaeosols (e.g. Kraus & Hasiotis, 2006). For instance, stronger colors of palaeosols above sandstone bodies are attributed to better drainage conditions since the sandstone bodies commonly constitute the geomorphological highlands in the local. In general, a lower sedimentation rate and a longer hiatus contribute to a more developed soil profile, which is attributed to the more stable channel belt location (Kraus, 1999).

4.3 Distribution of sandstone bodies

The locations of FA3 and FA4 channel sandstone bodies are projected in the XY horizontal plane. Distributary channel deposits (FA1) are not projected because they are less geologically important, nor are large-scale, massive, trunk-shaped channel deposits (FA2) because of their relative scarcity (5 out of 92). Therefore, FA3 braided and FA4 sinuous channel sandstone bodies are the main focus, and they are observed to occur in a mixed manner (Figure 10). In other words, laterally (in the XY horizontal plane), FA3 braided or FA4 sinuous systems are not confined to certain portions of the study area, and they are rather mixed.

5. Discussion

Results from the integrated field analysis allow discussing the difference in flow conditions associated with sandstone bodies of different river styles. As mentioned in Section 4.3, the main focus of this study is on the FA3 (n = 48) and FA4 (n = 39) channel sandstone bodies, features of which point to braided and sinuous river styles, respectively. Nonetheless, the above interpretation of river styles is inevitably influenced by observations of the limited exposed outcrop. For instance, Holbrook & Allen (2021) report a case of a braided river that meanders, which means the above interpretations may be biased if only parts of the outcrop are observed. Moreover, since braided and sinuous rivers constitute a continuum in the river-flowing course, the study area may also be possibly situated in a transitional zone between sinuous- and braided-river-dominated zones, and thus the two main interpreted river systems may not be too far from each other. Therefore, it should be noted that the current interpretation is based on the available outcrop data and it may be slightly different if more data are available. In the later part of the discussion, efforts are made to explore controls on the geomorphic zonations and explain the mixture of river planform styles in the study area.

5.1 Bighorn Basin river styles and flow conditions

As discussed above, all the interpreted river styles are based on the best knowledge of the authors on the available outcrop data. Owing to the dominant abundance and geological importance, FA3 and FA4 deposits are the main targets for discussion.

FA3 braided channel sandstone deposits and FA4 sinuous channel sandstone deposits present both similarities and differences. First of all, the most dominant lithofacies in both of them is the planar cross-stratified sandstone (Sp; Figure 7E), which is the result of straight crested bedforms in the lower flow regime with intermittent to continuous sand motion and transcritical water flow conditions (Harms and Fahnestock, 1960; Coleman, 1969; Bourquin *et al.*, 2009; Went and McMahon, 2018). The second most dominant lithofacies in FA3 braided channel sandstone deposits is low-angle (<15°) cross-bedded sandstone (Sl), which is formed in upper flow regimes, accompanied by high sediment concentration and continuous sand motion (Harms and Fahnestock, 1960; Coleman, 1969; Bourquin *et al.*, 2009; Went and McMahon, 2018). In contrast, the second most dominant lithofacies in FA4 sinuous channel sandstone deposits is trough cross-stratified sandstone (St), which is the result of linguoid bedforms that mainly develop in the subcritical lower flow regimes. Based on the two most dominant lithofacies in FA3 and FA4, the flow velocity that produces FA3 braided channel sandstone deposits is in general higher than that produces FA4 sinuous channel sandstone deposits. From the perspective of Froude number (Kennedy, 1969), FA3 braided channel sandstone deposits should be formed in a condition of either higher velocity or shallower water depth or a combination of both than FA4 counterparts.

The narrow and thin single-story units in FA3 indicate short life-spans and quick lateral coalescence of multiple channel stories that may result from multiple phases of ephemeral flow (Gibling, 2006) or spike-like discharge conditions (Fielding *et al.*, 2018). In contrast, the presence of lateral accretional surfaces and the sinuosity index up to 1.8 (Figs. 8 and S2) in FA4 suggest more stable, perennial water flow conditions. More importantly, FA3 braided channel deposits are significantly thinner and insignificantly narrower than

FA4 sinuous channel deposits, which indicates FA3 may be formed in flashy-discharge conditions instead of continuously high-discharge conditions (Fielding *et al.*, 2018).

The insignificant difference in paleoflow directions between FA3 and FA4 suggests that they may have developed in channel belts with similar downstream orientation. Measurements of palaeoflow directions in FA4 sinuous channel sandstone deposits are not uniform, and this is expected because they vary with the locations with reference to the meander bend and should show a large spread when plotted all together. Meanwhile, those in FA3 braided channel sandstone deposits are also different from the uniform distribution, and they have large circular deviation (standard deviation = 90°) and present dispersal pattern as the FA4 sinuous channel sandstone deposits do (standard deviation = 98°). Pryor (1960) suggested that the slope of the depositional surface is the most important factor controlling the circular deviation and dispersal pattern of the paleoflow data, with a larger slope contributing to more uniform paleoflow data. Therefore, it can be inferred that the slope was gentle for both FA3 and FA4 deposition. In this context, discharge difference might be the main contributor to the river style change (Leopold & Wolman, 1957).

5.2 Geomorphic zonation of the Bighorn Basin

Literature shows that braided rivers evolve into sinuous rivers when certain thresholds in discharge and/or slope are exceeded (Leopold and Wolman, 1957; Bridge, 2003). As analyzed in the above section, the study area might be of a gentle slope during the deposition of FA3 and FA4, and thus the discharge condition may play a critical role in determining the river styles. The study area is far from the southern Owl Creek Mountains, and if it is the only catchment, sinuous rivers should develop in the study area according to the geomorphic zonation theory in river basins (Schumm, 1985). However, braided channel deposits do occur often (48 FA3 versus 39 FA4) in the study area. A hypothesis could be that there have been multiple feeding systems influencing the study area from the western catchments (Wing & Bown, 1985; Owen *et al.,* 2019). Given the proximity of the study area to the western catchment and the high gradient from the western basin margin relative to the southern and eastern margins in the early Eocene, the study area will likely have been fed by multiple western systems that confluence with an axial system flowing from south to north. Similar depositional models that include transverse and axial river systems have been reported in modern and ancient outcrop analogs as well as flume experiments (e.g. DeCelles *et al.*, 1991; DeCelles & Cavazza, 1999; Weissmann *et al.*, 2015, 2016; Giles *et al.*, 2016; Kim *et al.*, 2011; Connell *et al.*, 2012). The southern and eastern catchments are thought to have been lower and possibly more dominated by the reworking of Mesozoic fines (DeCelles *et al.*, 1991). With the feeding of basement-rich western source materials into the axial system of the basin, the sinuous systems may have been alternated or changed into braided systems downstream where discharge was temporarily increased.

The western Washakie Range, which is now covered by the Absaroka Mountains (Figure 2), was present during the deposition of the Willwood Formation, and it is hypothesized to be an important catchment for the transverse system (Owen *et al.*, 2019), which is supported by the presence of fanglomerates in the western margin of the basin (Kraus, 1984). Therefore, the river planform styles indicated by the rock records in the study area are the interfingering products of at least two river systems, namely one axial system and one transverse system. Accordingly, the paleogeography of the Bighorn Basin during the early Eocene is reconstructed (Figure 11). Detailed annotations of elements in this map are listed in the figure caption, with the information provided by existing literature and this study. The presented paleogeographic model represents one possible scenario where FA3 braided channel deposits are dominant in the study area during the period of high or ephemeral discharge conditions. There are some other scenarios when the study area hosts FA4 sinuous channel deposits, probably during the low/perennial discharge conditions based on the analysis in Section 5.1. To briefly summarize, water discharge in the main stream is determined by contributions from both axial and transverse systems at the upstream part of the study area, and high/ephemeral discharge conditions favor FA3 braided channel development while low/perennial discharge conditions favor FA4 sinuous channel development.

5.3 Controls on river styles and geomorphic zonation

River planform styles depend on several controlling conditions, including water discharge, transport material (bedload vs. suspended load), sediment concentration, valley gradient, and bank material strength (Schumm, 1985; Church, 2006). In an equilibrium-state river channel, sediment concentration is in balance with the valley gradient (Muto *et al.*, 2007; Wang *et al.*, 2021a). These controlling conditions are also influenced by upstream factors, and the sediment concentration can at times be greater than the transport capacity determined by valley gradient and stream power. When this happens, aggrading and braiding fluvial conditions tend to occur (Schumm, 1985; Church, 2006; Muto *et al.*, 2007). In contrast, the river will tend to entrain sediment and degrade when sediment concentration is lower than the transport capacity, and the preferred mode of transient degradation for the channel is to become more sinuous until the channel gradient is reduced to the required value (Bettess & White 1983), unless bank strength prevents it from reaching the equilibrium gradient (Church, 2006). Therefore, the climatically-controlled sediment concentration can lead to river style change by shifting the geomorphic zonation boundaries between two adjacent river styles towards upstream or downstream directions (Holbrook *et al.*, 2006).

The early Eocene river systems in the Bighorn Basin experienced strong climate alternations likely driven by orbital forcing (Abels *et al.*, 2013), and these climate alternations may be embodied by changes in temperature, precipitation, vegetation cover, bank erodibility, suspended load/bedload ratio, and seasonal contrast (Vandenberghe, 1995, 2003). It is anticipated that some other proxies may provide constraints for inference of the above-mentioned climate alternations, particularly the hydrodynamic conditions. However, sandbody data are not yet integrated with other proxies, such as paleosol data, in the Bighorn Basin studies towards paleoclimatic reconstruction. Therefore, a detailed stratigraphic analysis is needed to stratigraphically and statistically establish a possible precession- or eccentricity-scale relation between floodplain aggradational cycles (cf. Wang *et al.*, 2021b) and sandstone bodies of different river styles to improve the climatic reconstruction in the Bighorn Basin.

6. Conclusions

In this study, a comprehensive sedimentological analysis is carried out on outcrops of the lower Eocene Willwood Formation in the Bighorn Basin, USA, using both field-documented data and UAV-photogrammetric model measurements. A total of four channel lithofacies associations are recognized, which are interpreted to be deposits of four river planform styles: distributary channel, massive trunk-shaped channel, braided channel, and sinuous channel, respectively, with the latter two styles as dominant ones. Braided and sinuous channel sandstone bodies differ significantly in thicknesses (on average 6.1 m versus 9.0 m) and insignificantly in widths (on average 231 m) and paleoflow directions (on average N003). They are different in lithofacies compositions, but planar cross-stratified sandstone is the most dominant lithofacies in both types of deposits. The alternating presence of sinuous and braided river styles recorded in the outcrop offer insights towards the reconstruction of a palaeogeographic model for the early Eocene period. In the schematized model, several transverse systems confluence with an axial system roughly following the basin axis. Contributions from both transverse and axial systems determine water discharge and sediment supply in the channel belt and thus the river style. Findings from this study suggest that channel sandstone body data can be undertaken in the integrated analysis to improve paleoclimatic reconstruction in the Bighorn Basin.

Acknowledgements

This study was financially supported by Top Sectors GeoEnergie, Equinor, and Wintershall to HAA, JEAS, AWM, and TFB (FRESCO Project, Grant No. TKI2018–03–GE), China Scholarship Council to YW (No. 201606440046), the Dutch Molengraaff fund (Stichting Molengraaff Fonds) to YW, and the IAS/SEPM travel grant to YW. Scott Wing is thanked for constructive comments on the Bighorn Basin paleogeomorphology. The authors acknowledge the help from Chaowen Wang, Dirk-Jan Walstra, and the Churchill family of Wyoming.

Conflicts of Interest

The authors declare no conflicts of interest in preparing this manuscript.

Data Availability

The data that support the findings of this study are available from the corresponding author upon request.

References

Abdul Aziz, H., **Hilgen, F.J.**, **van Luijk, G.M.**, **Sluijs, A.**, **Kraus, M.J.**, **Pares, J.M.** and **Gingerich, P.D.** (2008) Astronomical climate control on paleosol stacking patterns in the upper Paleocene–lower Eocene Willwood Formation, Bighorn Basin, Wyoming. *Geology*, **36**, 531.

Abels, H.A., **Clyde, W.C.**, **Gingerich, P.D.**, **Hilgen, F.J.**, **Fricke, H.C.**, **Bowen, G.J.** and **Lourens, L.J.** (2012) Terrestrial carbon isotope excursions and biotic change during Palaeogene hyperthermals. *Nature Geosci*, **5**, 326–329.

Abels, H.A., **Kraus, M.J.** and **Gingerich, P.D.** (2013) Precession-scale cyclicity in the fluvial lower Eocene Willwood Formation of the Bighorn Basin, Wyoming (USA). *Sedimentology*, **60**, 1467–1483.

Abels, H.A., **Lauretano, V.**, **van Yperen, A.E.**, **Hopman, T.**, **Zachos, J.C.**, **Lourens, L.J.**, **Gingerich, P.D.** and **Bowen, G.J.** (2016) Environmental impact and magnitude of paleosol carbonate carbon isotope excursions marking five early Eocene hyperthermals in the Bighorn Basin, Wyoming. *Clim. Past*, **12**, 1151–1163.

Agarwal, R.P. and **Bhoj, R.** (1992) Evolution of Kosi river fan, India: structural implications and geomorphic significance. *International Journal of Remote Sensing*, **13**, 1891–1901.

Allen, J.P., **Fielding, C.R.**, **Gibling, M.R.** and **Rygel, M.C.** (2013) Recognizing products of palaeoclimate fluctuation in the fluvial stratigraphic record: An example from the Pennsylvanian to Lower Permian of Cape Breton Island, Nova Scotia. *Sedimentology*, **61**, 1332–1138.

Allen, J.R.L. (1978) Studies in fluviatile sedimentation: an exploratory quantitative model for the architecture of avulsion-controlled alluvial suites. *Sedimentary Geology*, **21**, 129–147.

Aziz, H.A., **Hilgen, F.J.**, **van Luijk, G.M.**, **Sluijs, A.**, **Kraus, M.J.**, **Pares, J.M.** and **Gingerich, P.D.** (2008) Astronomical climate control on paleosol stacking patterns in the upper Paleocene–lower Eocene Willwood Formation, Bighorn Basin, Wyoming. *Geology*, **36**, 531.

Bettess, R. and **White, W.R.** (1983) Meandering And Braiding Of Alluvial Channels. *Proceedings of the Institution of Civil Engineers*, **75**, 525–538.

Bijkerk, J.F., **ten Veen, J.**, **Postma, G.**, **Mikeš, D.**, **van Strien, W.** and **de Vries, J.** (2014) The role of climate variation in delta architecture: lessons from analogue modelling. *Basin Res.*, **26**, 351–368.

Birgenheier, L., **Vanden Berg, M.**, **Plink-Bjorklund, P.**, **Gall, R.**, **Rosencrans, E.**, **Rosenberg, M.J.**, **Toms, L.C.** and **Morris, J.** (2019) Climate impact on fluvial-lake system evolution, Eocene Green River Formation, Uinta Basin, Utah, USA. GSA Bulletin. doi: 10.1130/B31808.1

Blackstone, D.L. (1940) Structure of the Pryor Mountains Montana. *The Journal of Geology*, **48**, 590–618.

Bourquin, S., **Guillocheau, F.** and **Péron, S.** (2009) Braided rivers within an arid alluvial plain (example from the Lower Triassic, western German Basin): recognition criteria and expression of stratigraphic cycles. Sedimentology. doi: 10.1111/j.1365-3091.2009.01078.x

Bown, T. M. (1980) Summary of latest Cretaceous and Cenozoic sedimentary, tectonic and erosional events, Bighorn Basin, Wyoming. In: P. D. Gingerich (Editor), Early Cenozoic Paleontology and Stratigraphy of the Bighorn Basin, Wyoming. *Univ. Mich. Pap. Paleontol.*, **24**, 25-32.

Bradley, R. W. and **Venditti, J. G.** (2017) Reevaluating dune scaling relations. *Earth-Sci. Rev.*, **165**, 356–376.

Bridge, J.S. (1993) The interaction between channel geometry, water flow, sediment transport and deposition in braided rivers. *Geological Society, London, Special Publications*, **75**, 13–71.

Bridge, J.S. and **Leeder, M.R.** (1979) A simulation model of alluvial stratigraphy. *Sedimentology*, **26**, 617–644.

Bridge, J.S. and **Tye, B.** (2000) Interpreting the dimensions of ancient fluvial channel bars, channels, and channel belts from wireline-logs and cores. *AAPG Bulletin*, **84**, 1205–1228.

Bryant, I., **Carr, D.**, **Cirilli, P.**, **Drinkwater, N.**, **McCormick, D.**, **Tilke, P.** and **Thurmond, J.** (2000) Use of 3D digital analogues as templates in reservoir modelling. *Petroleum Geoscience,* **6**, 195–201.

Buckley, S.J., **Ringdal, K.**, **Naumann, N.**, **Dolva, B.**, **Kurz, T.H.**, **Howell, J.A.** and **Dewez, T.J.B.** (2019) LIME: Software for 3-D visualization, interpretation, and communication of virtual geoscience models. *Geosphere*, **15**, 222–235.

Church, M. (2006) Bed material transport and the morphology of alluvial river channels. *Annu. Rev. Earth Planet. Sci.*, **34**, 325–354.

Clyde, W., **Stamatakos, J.** and **Gingerich, P.** (1994) Chronology of the Wasatchian Land-Mammal Age (Early Eocene): Magnetostratigraphic Results from the McCullough Peaks Section, Northern Bighorn Basin, Wyoming. *Journal of Geology*, **102**, 367-377.

Clyde, W.C. and **Christensen** (2003) Testing the relationship between pedofacies and avulsion using Markov analysis. *American Journal of Science*, **303**, 60–71.

Coleman, J.M. (1969) Brahmaputra river: Channel processes and sedimentation. *Sedimentary Geology*, **3**, 129–239.

Colombera, L., **Arévalo, O.J.** and **Mountney, N.P.** (2017) Fluvial-system response to climate change: The Paleocene-Eocene Tremp Group, Pyrenees, Spain. *Global and Planetary Change*, **157**, 1–17.

Colombera, L., **Mountney, N.P.**, **Howell, J.A.**, **Rittersbacher, A.**, **Felletti, F.** and **McCaffrey, W.D.** (2016) A test of analog-based tools for quantitative prediction of large-scale fluvial architecture. *Bulletin*, **100**, 237–267.

Connell, S. D., Kim, W., Paola, C., & Smith, G. A. (2012). Fluvial Morphology and Sediment-Flux Steering of Axial-Transverse Boundaries In An Experimental Basin. *Journal of Sedimentary Research*, **82**, 310–325.

Davies-Vollum, K.S. and **Wing, S.L.** (1998) Sedimentological, Taphonomic, and Climatic Aspects of Eocene Swamp Deposits (Willwood Formation, Bighorn Basin, Wyoming). *PALAIOS*, **13**, 28.

DeCelles, P.G. and **Cavazza, W.** (1999) A comparison of fluvial megafans in the Cordilleran (Upper Cretaceous) and modern Himalayan foreland basin systems. *Geological Society of America Bulletin*, **20**.

DeCelles, P.G., **Gray, M.B.**, **Ridgway, K.D.**, **Cole, R.B.**, **Pivnik, D.A.**, **Pequera, N.** and **Srivastava, P.** (1991) Controls on synorogenic alluvial-fan architecture, Beartooth Conglomerate (Palaeocene), Wyoming and Montana. *Sedimentology*, **38**, 567–590.

Eltner, A., **Kaiser, A.**, **Castillo, C.**, **Rock, G.**, **Neugirg, F.** and **Abellan, A.** (2016) Image-based surface reconstruction in geomorphometry - merits, limits and developments. *Earth Surface Dynamics,* **4**, 359–389.

Enge, H.D., **Buckley, S.J.**, **Rotevatn, A.** and **Howell, J.A.** (2007) From outcrop to reservoir simulation model: Workflow and procedures. *Geosphere*, **3**, 469.

Fabuel-Perez, I., Hodgetts, D. & Redfern, J. (2009) A new approach for outcrop characterization and geostatistical analysis of a low-sinuosity fluvial-dominated succession using digital outcrop models:

Upper Triassic Oukaimeden Sandstone Formation, central High Atlas, Morocco. *American Association of Petroleum Geologists Bulletin*, **93**, 795–827.

Fielding, C.R., **Alexander, J.** and **Allen, J.P.** (2018) The role of discharge variability in the formation and preservation of alluvial sediment bodies. *Sedimentary Geology*, **365**, 1–20.

Fielding, C.R., **Ashworth, P.J.**, **Best, J.L.**, **Prokocki, E.W.** and **Smith, G.H.S.** (2012) Tributary, distributary and other fluvial patterns: What really represents the norm in the continental rock record? *Sedimentary Geology*, **261–262**, 15–32.

Fisher, J. A., Nichols, G. J. and Waltham, D. A. (2007). Unconfined flow deposits in distal sectors of fluvial distributary systems: Examples from the Miocene Luna and Huesca Systems, northern Spain, *Sedimentary Geology*, **195**, 55–73.

Foose, R.M., **Wise, D.U.** and **Garbarini, G.S.** (1961) Structural Geology of the Beartooth Mountains, Montana and Wyoming. *Geol Soc America Bull*, **72**, 1143.

Foreman, B.Z. (2014) Climate-driven generation of a fluvial sheet sand body at the Paleocene-Eocene boundary in north-west Wyoming (USA). *Basin Res*, **26**, 225–241.

Foreman, B.Z., **Heller, P.L.** and **Clementz, M.T.** (2012) Fluvial response to abrupt global warming at the Palaeocene/Eocene boundary. *Nature*, **491**, 92–95.

Ghinassi, M., **Ielpi, A.**, **Aldinucci, M.** and **Fustic, M.** (2016) Downstream-migrating fluvial point bars in the rock record. *Sedimentary Geology*, **334**, 66–96.

Ghinassi, M. and **Ielpi, A.** (2018) Morphodynamics and facies architecture of streamflow-dominated, sand-rich alluvial fans, Pleistocene Upper Valdarno Basin, Italy. *Geol. Soc. Lond. Spec. Publ.*, **440**, 175–200.

Gibling, M.R. (2006) Width and thickness of fluvial channel bodies and valley fills in the geological record: a literature compilation and classification. *Journal of Sedimentary Research*, **76**, 731–770.

Giles, P., **Whitehouse, B.** and **Karymbalis, E.** (2016) Interactions between alluvial fans and axial rivers in Yukon, Canada and Alaska, USA. In: Ventra, D. & Clarke, L.E. (eds) Geology and Geomorphology of Alluvial and Fluvial Fans: Terrestrial and Planetary Perspectives. *Geological Society, London, Special Publications*, **440**.

Gingerich, P.D. (1983) Paleocene-Eocene faunal zones and a preliminary analysis of Laramide structural deformation in the Clark's Fork Basin, Wyoming. In 34th Annual Field Conference, *Wyoming Geological Association Guidebook*, pp. 185–195.

Gingerich, P. D. (2010) Mammalian faunal succession through the Paleocene-Eocene thermal maximum (PETM) in western North America**.** *Vertebrata PalAsiatica*, **48**, 308–327**.**

Gradstein, F.M., Ogg, J.G., Schmitz, M.D., and **Ogg, G.M.** (2012) The Geologic Time Scale 2012, Amsterdam, The Netherlands, Elsevier.

Hajek, E.A., **Heller, P.L.** and **Sheets, B.A.** (2010) Significance of channel-belt clustering in alluvial basins. *Geology*, **38**, 535–538.

Hajek, E.A. and **Wolinsky, M.A.** (2012) Simplified process modeling of river avulsion and alluvial architecture: Connecting models and field data. *Sedimentary Geology*, **257–260**, 1–30.

Hampson, G.J., **Jewell, T.O.**, **Irfan, N.**, **Gani, M.R.** and **Bracken, B.** (2013) Modest Change In Fluvial Style With Varying Accommodation In Regressive Alluvial-To-Coastal-Plain Wedge: Upper Cretaceous Blackhawk Formation, Wasatch Plateau, Central Utah, U.S.A. *Journal of Sedimentary Research*, **83**, 145–169.

Hartley, A.J., **Weissmann, G.S.**, **Nichols, G.J.** and **Warwick, G.L.** (2010) Large Distributive Fluvial Systems: Characteristics, Distribution, and Controls on Development. *Journal of Sedimentary Research*, **80**, 167–183.

Harms, J.C. and Fahnestock, R.K. (1965) Stratification, bed forms and flow phenomena (with an example from the Rio Grande). G.V. Middleton (Ed.), Primary Sedimentary Structures and their Hydrodynamics Interpretation, *Soc. Econ. Paleontol. Mineral., Spec. Publ.*, **12**, 84-115.

Holbrook, J., **Scott, R.W.** and **Oboh-Ikuenobe, F.E.** (2006) Base-Level Buffers and Buttresses: A Model for Upstream Versus Downstream Control on Fluvial Geometry and Architecture Within Sequences. *J. Sediment. Res.*, **76**, 162–174.

Holbrook, J.M. and **Allen, S.D.** (2021) The case of the braided river that meandered: Bar assemblages as a mechanism for meandering along the pervasively braided Missouri River, USA. *GSA Bull.*, **133**, 1505–1530.

Howell, J.A., Martinius, A.W. and **Good, T.R.** (2014) The application of outcrop analogues in geological modelling: a review, present status and future outlook. *Geol. Soc. Lond. Spec. Publ.*, **387**, 1–25.

Jerolmack, D.J. and **Paola, C.** (2007) Complexity in a cellular model of river avulsion. *Geomorphology*, **91**, 259–270.

Karssenberg, D. and **Bridge, J.S.** (2008) A three-dimensional numerical model of sediment transport, erosion and deposition within a network of channel belts, floodplain and hill slope: extrinsic and intrinsic controls on floodplain dynamics and alluvial architecture. *Sedimentology*, **55**, 1717–1745.

Kennedy, J. F. (1969) The formation of sediment ripples, dunes and antidunes. *Annu. Rev. Fluid Mech.*, **1**, 147.

Kim, W., **Connell, S.D.**, **Steel, E.**, **Smith, G.A.** and **Paola, C.** (2011) Mass-balance control on the interaction of axial and transverse channel systems. *Geology*, **39**, 611–614.

Kraus, M.J. (1983) Genesis of early Tertiary exotic metaquartzite conglomerates in the western Bighorn Basin, northwest Wyoming. PhD Thesis, University of Colorado, Boulder.

Kraus, M.J. (1984) Sedimentology and tectonic setting of early Tertiary quartzite conglomerates, northwest Wyoming, in Koster, E.H., and Steel, R.J., eds., Sedimentology of gravels and conglomerates. *Canadian Society of Petroleum Geologists Memoir*, **10**, 203–216.

Kraus, M.J. (1985) Sedimentology of early Tertiary rocks, northern Bighorn Basin. In: *Field Guidebook to Modern and Ancient Fluvial Systems in the United States: Proceedings* (Ed. by R.M. Flores &M. Harvey) *Third International Fluvial Sedimentology Conference*, 26–33.

Kraus, M.J. (1999) Paleosols in clastic sedimentary rocks: their geologic applications. *Earth-Science Reviews*, **47**, 41–70.

Kraus, M.J. (2002) Basin-Scale Changes in Floodplain Paleosols: Implications for Interpreting Alluvial Architecture. *Journal of Sedimentary Research*, **72**, 500–509.

Kraus, M.J. and **Aslan, A.** (1993) Eocene Hydromorphic Paleosols: Significance for Interpreting Ancient Floodplain Processes. *Journal of Sedimentary Petrology*, **63**, 453–463.

Kraus, M.J. and **Davies-Vollum, K.S.** (2004) Mudrock-dominated fills formed in avulsion splay channels: examples from the Willwood Formation, Wyoming. *Sedimentology*, **51**, 1127–1144.

Kraus, M.J. and **Gwinn, B.** (1997) Facies and facies architecture of Paleogene floodplain deposits, Willwood Formation, Bighorn Basin, Wyoming, USA. *Sedimentary Geology*, **114**, 33–54.

Kraus, M.J. and **Hasiotis, S.T.** (2006) Significance of different modes of rhizolith preservation to interpreting paleoenvironmental and paleohydrologic settings: examples from Paleogene paleosols, Bighorn Basin, Wyoming, U.S.A. *Journal of Sedimentary Research*, **76**, 633-646.

Kraus, M.J. and Middleton, L. (1987) Contrasting architecture of two alluvial suites in different structural settings. In: F.G. Ethridge, R.M. Fiores and M.D. Harvey (Editors). *Recent Developments in Fluvial Sedimentology. SEPM Spec. Pubi.*, **39**, 253-262.

Leclair, S.F. and **Bridge, J.S.** (2001) Quantitative interpretation of sedimentary structures formed by river dunes. *Journal of Sedimentary Research*, **71**, 713–716.

Leopold, L.B. and **Wolman, M.G.** (1957) River channel patterns: braided, meandering and straight, *US Geological Survey Professional Paper*, **282-B**, pp. 85.

Lillegraven, J.A. and **Ostresh, L.M., Jr.** (1988) Evolution of Wyoming's early Cenozoic topography and drainage patterns: National Geographic Research, **4**, p. 303–327.

Lillegraven, J.A. (2009) Where was the western margin of northwestern Wyoming's Bighorn Basin late in the early Eocene? In: *Papers on Geology, Vertebrate Paleontology, and Biostratigraphy in Honor of Michael O. Woodburne* (Ed. By L.B. Albright, III), *Mus. Northern Arizona Bull.*, **65**, 37 – 82.

Mackey, S.D. and **Bridge, J.S.** (1995) Three-Dimensional Model of Alluvial Stratigraphy: Theory and Application. *Journal of Sedimentary Research*, **65**, 7–31.

Manna, M.O., **Scherer, C.M. dos S.**, **Bállico, M.B.**, **Reis, A.D. dos**, **Moraes, L.V.**, **Ferrari, L.A.B.**, **Roisenberg, H.B.** and **Oliveira, V.G. de** (2021) Changes in fluvial architecture induced by discharge variability, Jaicós Formation (Silurian-Devonian), Parnaíba Basin, Brazil. *Sedimentary Geology*, **420**, 105924.

Martinius, A.W. (2000) Labyrinthine Facies Architecture of the Tortola Fluvial System and Controls on Deposition (Late Oligocene-Early Miocene, Loranca Basin, Spain). *Journal of Sedimentary Research*, **70**, 850–867.

McBride, E.F. (1963) A Classification of Common Sandstones. *J. Sed. Petrol.*, **33**, 664–669.

Miall, A.D. (1985) Architectural-element analysis: a new method of facies analysis applied to fluvial deposits. *Earth Science Reviews*, **22**, 261-308

Miall, A.D. (1996) The Geology of Fluvial Deposits (Sedimentrary Facies. Basin Analysis, and Petroleum Geology). *Springer-verlag, New York*, 565.

Mohrig, D., **Heller, P.L.**, **Paola, C.** and **Lyons, W.J.** (2000) Interpreting avulsion process from ancient alluvial sequences: Guadalope-Matarranya system (northern Spain) and Wasatch Formation (western Colorado). *Geological Society of America Bulletin*, 17.

Muto, T., **Steel, R.** and **Swenson, J.** (2007) Autostratigraphy: A Framework Norm for Genetic Stratigraphy. *J. Sediment. Res.*, **77**, 2–12.

Neasham, J.W. (1967) The stratigraphy of the Willwood Formation in the vicinity of Sheep Mountain, southwestern Bighorn County, Wyoming. *Master Thesis*, *Iowa State University*, pp. 74.

Neasham J.W. (1970) Sedimentology of the Willwood Formation (lower Eocene): an alluvial molasse facies in northwestern Wyoming. *Ph.D. Thesis*, *Iowa State University*, pp. 98.

Neasham, J.W. and **Vondra, C.F.** (1972) Stratigraphy and Petrology of the Lower Eocene Willwood Formation, Bighorn Basin, Wyoming. *Geol Soc America Bull*, **83**, 2167.

Owen, A., **Ebinghaus, A.**, **Hartley, A.J.**, **Santos, M.G.M.** and **Weissmann, G.S.** (2017) Multi-scale classification of fluvial architecture: An example from the Palaeocene-Eocene Bighorn Basin, Wyoming. *Sedimentology*, **64**, 1572–1596.

Owen, A., **Hartley, A.J.**, **Ebinghaus, A.**, **Weissmann, G.S.** and **Santos, M.G.M.** (2019) Basin-scale predictive models of alluvial architecture: Constraints from the Palaeocene-Eocene, Bighorn Basin, Wyoming, USA. *Sedimentology*, **66**, 736–763.

Paredes, J.M., Foix, N.N. and Allard J.O. (2016) Sedimentology and alluvial architecture of the Bajo Barreal Formation (Upper Cretaceous) in the Golfo San Jorge Basin: outcrop analogues of the richest oil-bearing fluvial succession in Argentina. *Marine and Petroleum Geology*, **72**, 317-335.

Posamentier, H., **Davies, R.**, **Cartwright, J.** and **Wood, L.** (2007) Seismic geomorphology - An overview. *Geological Society, London, Special Publications*, **277**, 1–14.

Pryor, W. A. (1960) Cretaceous sedimentation in Upper Mississipi embayment. *AAPG Bulletin*, **44**, 1473–1504.

Retallack, G.J. (2001) Soils of the Past: An Introduction to Paleopedology (2nd edn). *Blackwell Science*, Oxford, pp. 404.

Schumm, S.A. (1985) Patterns of alluvial rivers. *Annual Review of Earth and Planetary Sciences*, **13**, 5-27.

Scotese, C., **Song, H.**, **Mills, B.** and **Meer, D.** (2021) Phanerozoic Paleotemperatures: The Earth's Changing Climate during the Last 540 million years. Earth-Sci Rev. doi: 10.1016/j.earscirev.2021.103503

Shanley, K.W. and **McCabe, P.J.** (1994) Perspectives on the Sequence Stratigraphy of Continental Strata. *AAPG Bulletin*, **78 (4)**, 544–568.

Smedes, H.W. and **Prostka, H.J.** (1972) Stratigraphic framework of the Absaroka Volcanic Supergroup in the Yellowstone National Park region. *U.S. Geological Survey Professional Paper*, 729-C, 33 p.

Soil Survey Division Staff (1993) Soil Survey Manual, vol. 18. Soil Conservation Service, U.S. Department of Agriculture, USA.

Stap, L., **Sluijs, A.**, **Thomas, E.** and **Lourens, L.** (2009) Patterns and magnitude of deep sea carbonate dissolution during Eocene Thermal Maximum 2 and H2, Walvis Ridge, southeastern Atlantic Ocean. *Paleoceanography*, **24**, PA1211.

Sundell, K.A. (1990) Sedimentation and tectonics of the Absaroka Basin of northwestern Wyoming. In: Wyoming sedimentation and Tectonics, *41st Annual Field Conference Guidebook*, 105–122.

Szwarc, T.S., **Johnson, C.L.**, **Stright, L.E.** and **McFarlane, C.M.** (2015) Interactions between axial and transverse drainage systems in the Late Cretaceous Cordilleran foreland basin: Evidence from detrital zircons in the Straight Cliffs Formation, southern Utah, USA. *Geological Society of America Bulletin*, **127**, 372–392.

Valenza, J.M., **Edmonds, D.A.**, **Hwang, T.** and **Roy, S.** (2020) Downstream changes in river avulsion style are related to channel morphology. *Nature Communication*, **11**, 2116.

Varela, A.N. (2015) Tectonic control of accommodation space and sediment supply within the Mata Amarilla Formation (lower Upper Cretaceous) Patagonia, Argentina. *Sedimentology*, **62**, 867–896.

van den Berg, J.H, Martinius, A.W., and Houthuys, R. (2017) Breaching-Related Turbidites in Fluvial and Estuarine Channels: Examples from Outcrop and Core and Implications to Reservoir Models. *Marine and Petroleum Geology*, **82**, 178-205.

van der Meulen, B., **Gingerich, P.D.**, **Lourens, L.J.**, **Meijer, N.**, **van Broekhuizen, S.**, **van Ginneken, S.** and **Abels, H.A.** (2020) Carbon isotope and mammal recovery from extreme greenhouse warming at the Paleocene–Eocene boundary in astronomically-calibrated fluvial strata, Bighorn Basin, Wyoming, USA. *Earth Planet. Sci. Lett.*, **534**, 116044.

Vandenberghe, J. (1995) Timescales, climate and river development. *Quaternary Science Reviews*, **14**, 631–638.

Vandenberghe, J. (2003) Climate forcing of fluvial system development: an evolution of ideas. *Quaternary Science Reviews*, **22**, 2053–2060.

Vandenberghe, N., Hilgen, F.J., and Speijer, R.P. (2012) The Paleogene Period, in Gradstein, F.M., Ogg, J.G., Schmitz, M., and Ogg, G., eds., *The Geologic Time Scale 2012*, Amsterdam, The Netherlands, Elsevier, p. 855–921,

Wang, Y., **Baars, T.**, **Storms, J.**, **Martinius, A.**, **Gingerich, P.**, **Chmielewska, M.**, **Buckley, S.** and **Abels, H.** (2021a) Spatial characteristics and kinematics of precession-driven floodplain aggradation cycles in the lower Eocene Willwood Formation of the Bighorn Basin, Wyoming, USA. *Eartharxiv*, https://doi.org/10.31223/X5931M

Wang, Y., **Storms, J.E.A.**, **Martinius, A.W.**, **Karssenberg, D.** and **Abels, H.A.** (2021b) Evaluating alluvial stratigraphic response to cyclic and non-cyclic upstream forcing through process-based alluvial architecture modelling. *Basin Res.*, **33**, 48–65.

Weissmann, G.S., **Hartley, A.J.**, **Scuderi, L.A.**, **Nichols, G.J.**, **Owen, A.**, **Wright, S.**, **Felicia, A.L.**, **Holland, F.** and **Anaya, F.M.L.** (2015) Fluvial geomorphic elements in modern sedimentary basins and their potential preservation in the rock record: A review. *Geomorphology*, **250**, 187–219.

Wells, N.A. and **Dorr, J.A.** (1987) Shifting of the Kosi River, northern India. *Geology*, **15**, 204-207.

Went, D.J. and **McMahon, W.J.** (2018) Fluvial products and processes before the evolution of land plants: Evidence from the lower Cambrian Series Rouge, English Channel region. *Sedimentology*, **65**, 2559–2594.

Westerhold, T., **Marwan, N.**, **Drury, A.J.**, **Liebrand, D.**, **Agnini, C.**, **Anagnostou, E.**, **Barnet, J.S.K.**, **Bohaty, S.M.**, **De Vleeschouwer, D.**, **Florindo, F.**, **Frederichs, T.**, **Hodell, D.A.**, **Holbourn, A.E.**, **Kroon, D.**, **Lauretano, V.**, **Littler, K.**, **Lourens, L.J.**, **Lyle, M.**, **Pälike, H.**, **Röhl, U.**, **Tian, J.**, **Wilkens, R.H.**, **Wilson, P.A.** and **Zachos, J.C.** (2020) An astronomically dated record of Earth's climate and its predictability over the last 66 million years. *Science*, **369**, 1383–1387.

Westerhold, T., **Röhl, U.**, **Laskar, J.**, **Raffi, I.**, **Bowles, J.**, **Lourens, L.J.** and **Zachos, J.C.** (2007) On the duration of magnetochrons C24r and C25n and the timing of early Eocene global warming events: Implications from the Ocean Drilling Program Leg 208 Walvis Ridge depth transect. *Paleoceanography*, **22**, PA2201.

Whipple, K.X. and **Tucker, G.E.** (2002) Implications of sediment-flux-dependent river incision models for landscape evolution. *J. Geophys. Res.*, **107**, 2039.

Willett, S.D., **McCoy, S.W.**, **Perron, J.T.**, **Goren, L.** and **Chen, C.-Y.** (2014) Dynamic Reorganization of River Basins. *Science*, **343**, 1248765–1248765.

Williams, G.P. (1986) River meanders and channel size. *Journal of Hydrology*, **88**, 147–164.

Wing, S. and **Bown, T.M.** (1985) Fine Scale Reconstruction of Late Paleocene-Early Eocene Paleogeography in the Bighorn Basin of Northern Wyoming. In Flores, R., and Kaplan, S., eds., Cenozoic paleogeography of the west-central United States: Rocky Mountain Section, *Society of Economic Paleontologists and Mineralogists*, pp. 93–105.

Wise, D.U. (2000). Laramide Structures in Basement and Cover of the Beartooth Uplift Near Red Lodge, Montana. *AAPG Bulletin*, 84.

Yonkee, W.A. and **Weil, A.B.** (2015) Tectonic evolution of the Sevier and Laramide belts within the North American Cordillera orogenic system. *Earth-Science Reviews*, **150**, 531–593.

Yuretich, R.F., **Hickey, L.J.**, **Gregson, B.P.** and **Hsia, Y.L.** (1984) Lacustrine Deposits in the Paleocene Fort Union Formation, Northern Bighorn Basin, Montana. *J. Sed. Petrol.*, **54**, 836–852.

Zachos, J.C., McCarren, H., Murphy, B., Röhl, U., and Westerhold, T. (2010) Tempo and scale of late Paleocene and early Eocene carbon isotope cycles: Implications for the origin of hyperthermals. *Earth and Planetary Science Letters*, **299**, 242–249.

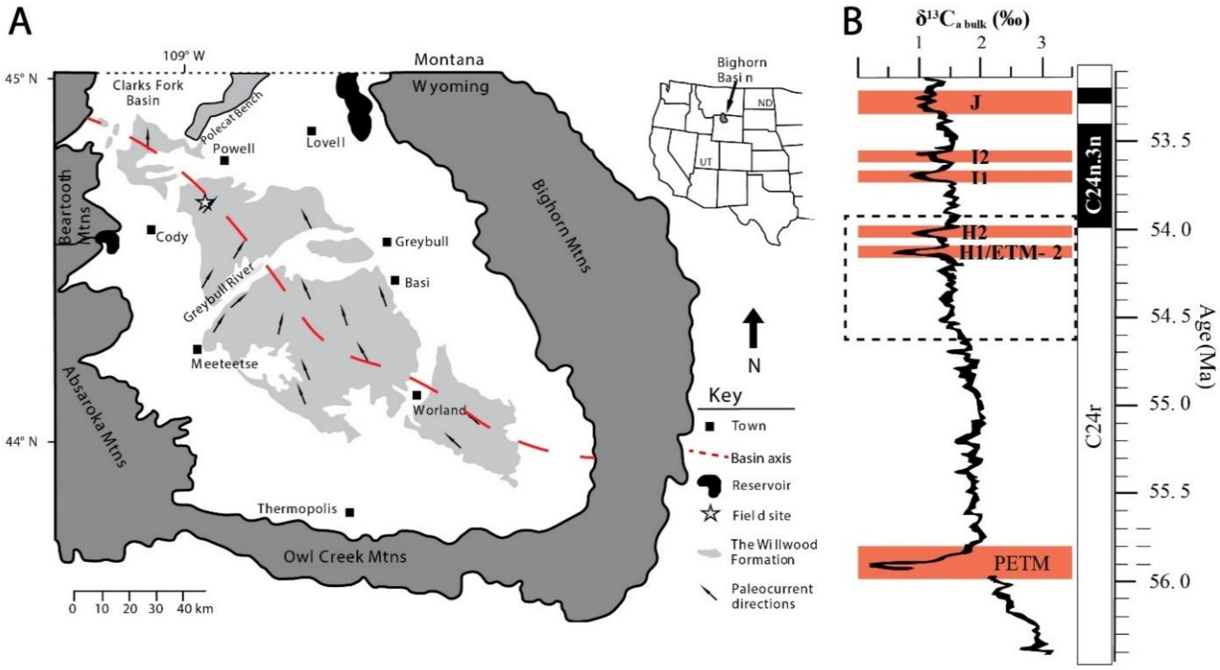

Figure 1. (A) The location of the study area, the McCullough Peaks, in the northern Bighorn Basin, Wyoming, USA (after Wang *et al.*, 2018), with basin axis following Finn *et al.* (2010). (B) Adjusted $\delta^{13}C_{a\ bulk}$ data from Zachos *et al.* (2010) to Gradstein *et al.* (2012) global timescale (Vandenberghe *et al.*, 2012) by Birgenheier *et al.* (2019), with orange rectangles indicating hyperthermal events and the dashed rectangle indicating the study interval.

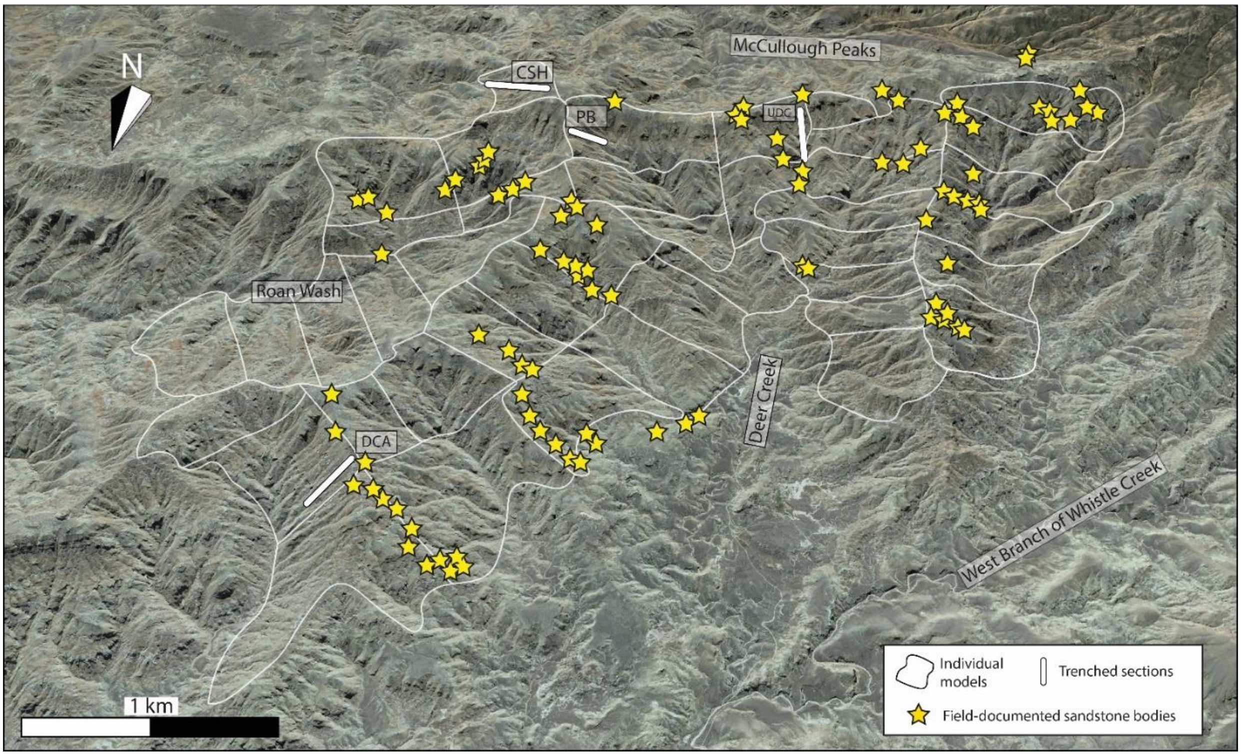

Figure 2. Bird's eye view from Google Earth showing UAV-based photogrammetric model coverage and field-documented sandstone bodies. Abbreviations: DCA--Deer Creek Amphitheater section (Abels *et al.*, 2013), UDC--Upper Deer Creek section (Abels *et al.*, 2012), CSH--Creek Star Hill section (Abels *et al.*, 2016), and PB--Purple Butte section.

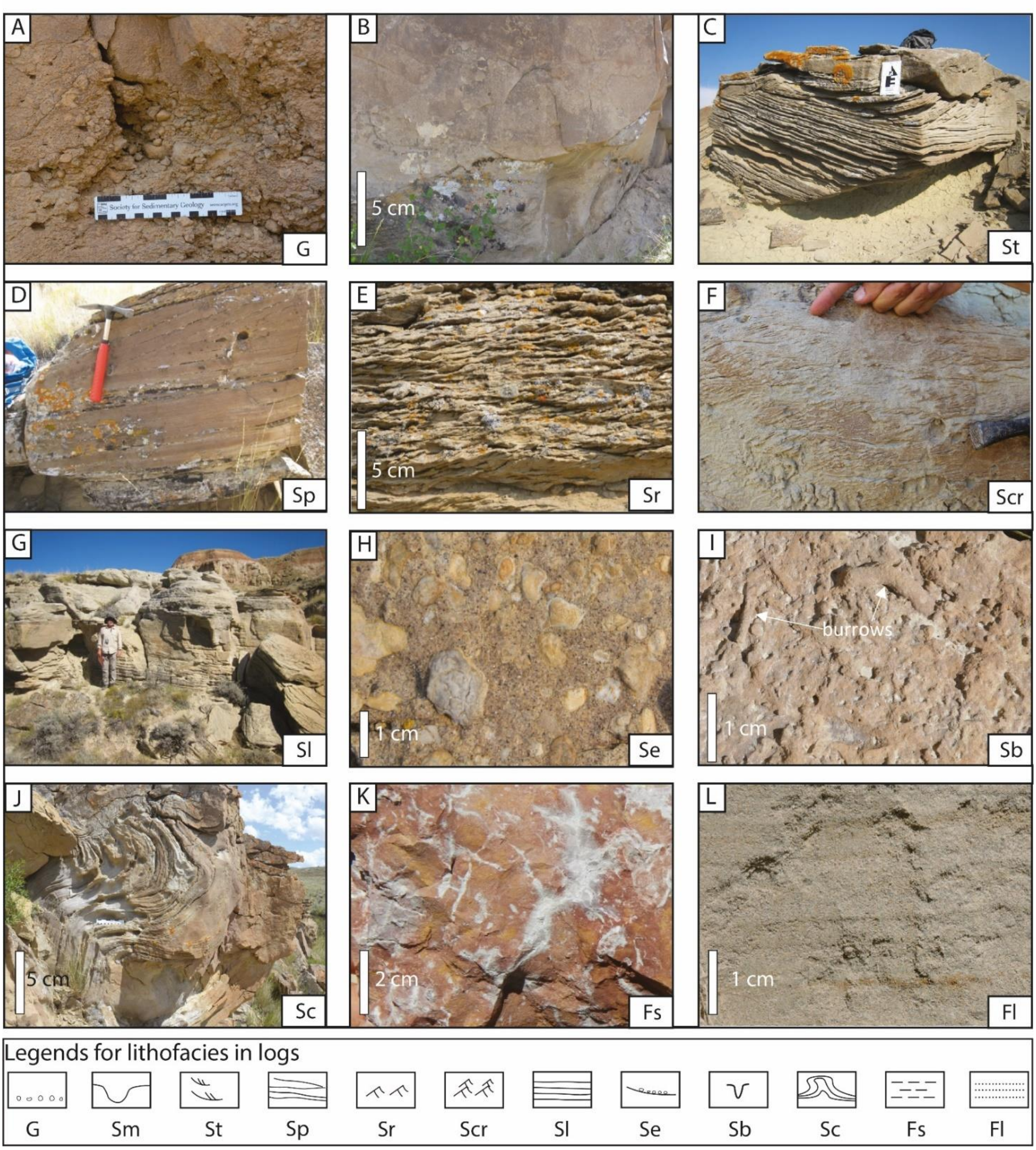

Figure 3. Lithofacies recognized in the study area. A. Clast-supported conglomerate (lithofacies G); scale bar length = 15 cm. B. Massive sandstone (lithofacies Sm). C. Trough cross-stratified sandstone (St); card length = 10 cm. D. Planar/Tabular cross-stratified sandstone (lithofacies Sp); hammer length = 25 cm. E. Ripple cross-laminated sandstone (lithofacies Sr). F. Climbing-ripple cross-laminated sandstone (lithofacies Scr). G. Low-angle (<15°) cross-bedded sandstone (lithofacies Sl); person height = 180 cm. H. Sandstone with erosional scour and fill (lithofacies Se), with floating carbonate nodules as the lag deposits. I. Bioturbated sandstone (lithofacies Sb). J. Convoluted sandstone (lithofacies Sc). K. Mudstones and siltstones (lithofacies Fs). L. Laminated siltstones (lithofacies Fl). Legends for lithofacies are shown for logs in the below figures.

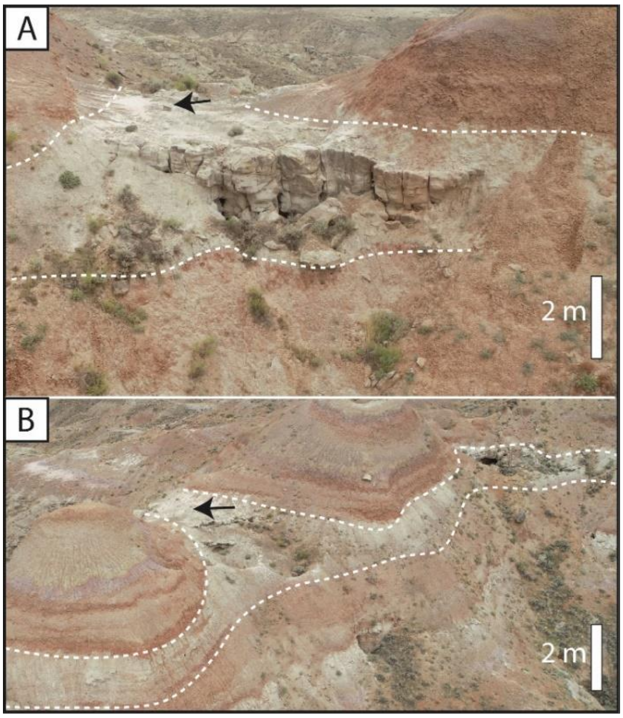

Figure 4. Facies Association 1: small-scale cut-and-fill channel sandstone deposit. (A) UAV photo showing the channel body in transverse view. (B) UAV photo showing the ribbon shape of the same channel body in longitudinal view. The two black arrows in subfigures A and B point at the same gravel rock debris on the ground.

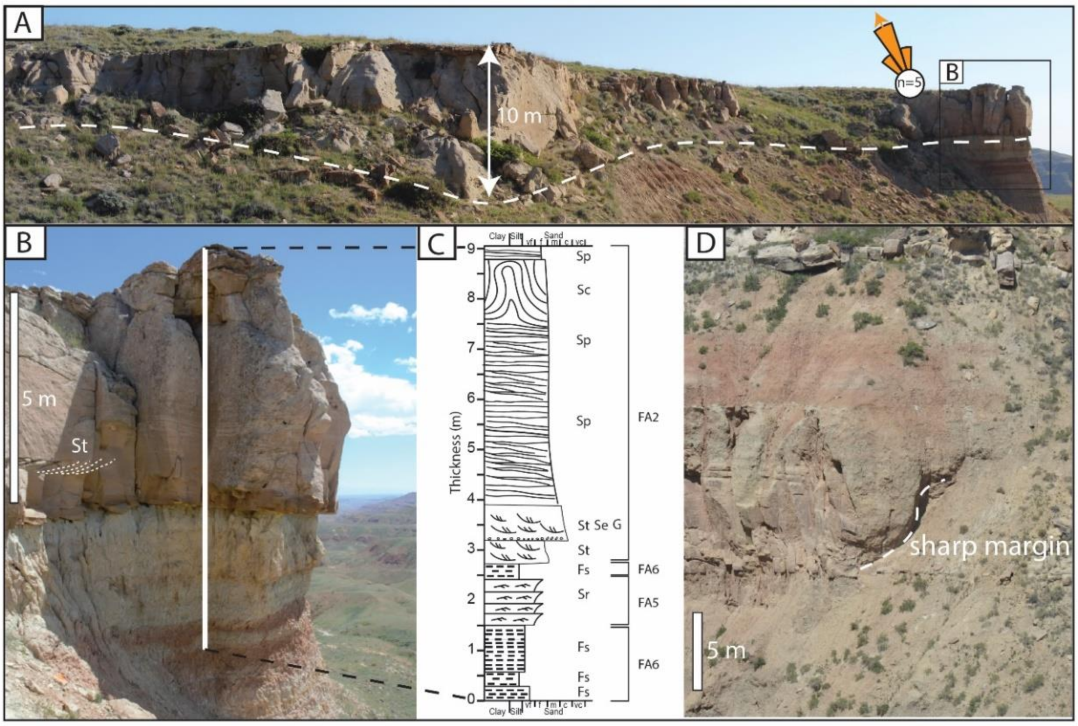

Figure 5. Facies Association 2: large-scale, massive, trunk-shaped channel sandstone deposit. (A) Overview of the large-scale, massive trunk-shaped channel deposits with a maximum thickness of ~10 m. (B–C) Zoomed-in view and log of the right side of subfigure A showing detailed sedimentary structures and underlying floodplain fines. The white line marks the corresponding sedimentological log position. (D) A second example of FA2 deposits that have a maximum thickness of ~10 m with sharp channel margins eroding into floodplain fines and a thin splay bed in the lower part. For legend, see Figure 3.

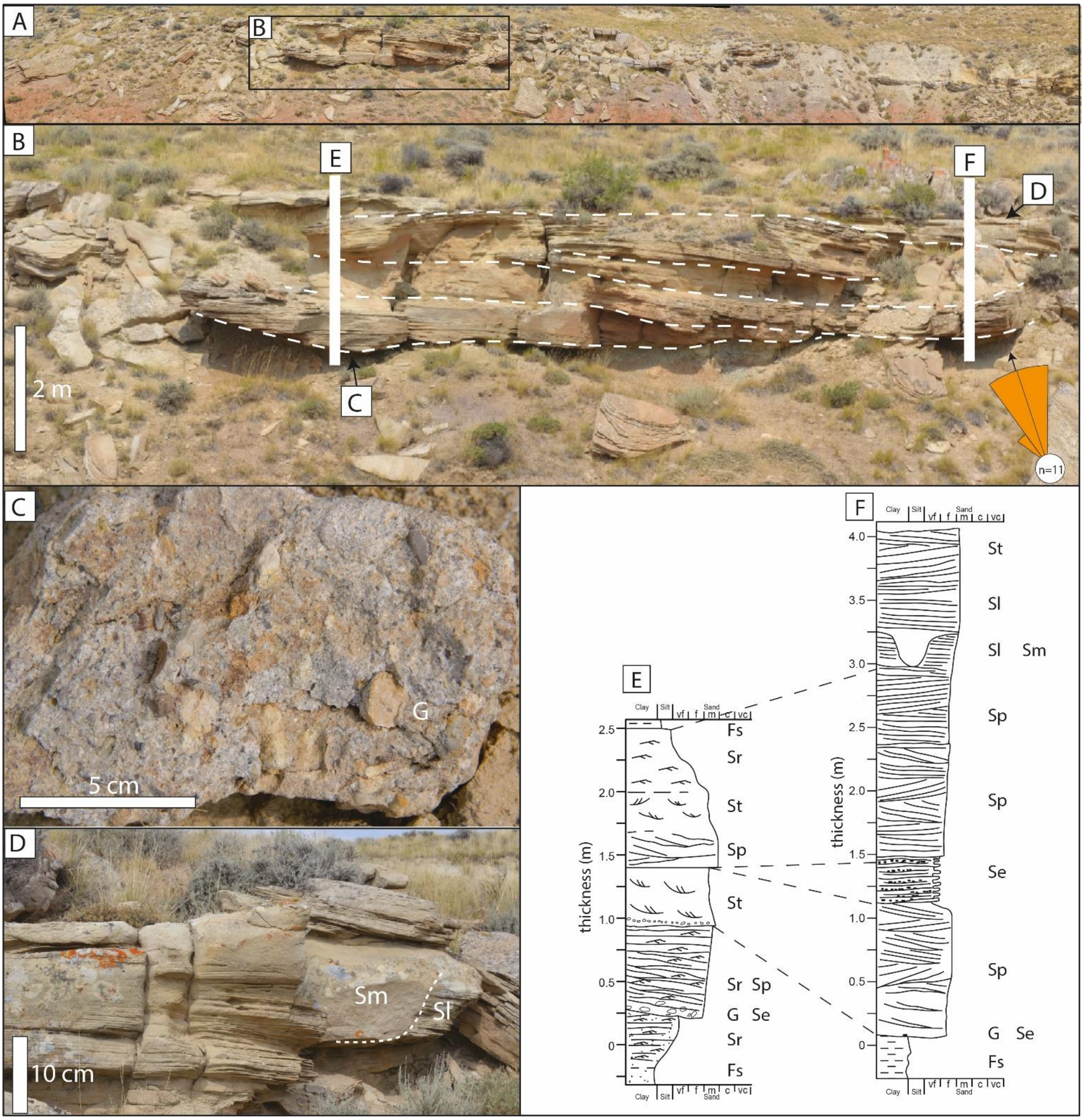

Figure 6. Facies Association 3: braided channel sandstone deposits. (A–B) Overview and close-up view of FA3 deposits, where there are five stories with the thickness of each varying between 0.5 and 1 m. (C) The bottom view of the channel base with floodplain nodules as lag deposits. (D) Massive bank-breaching deposits (Sm; cf. Van den Berg *et al.*, 2017) eroding low-angle cross-bedded sandstone (Sl). (E–F) Sedimentary logs for locations in panel B, showing the vertical succession of lithofacies in FA3. For legend, see Figure 3.

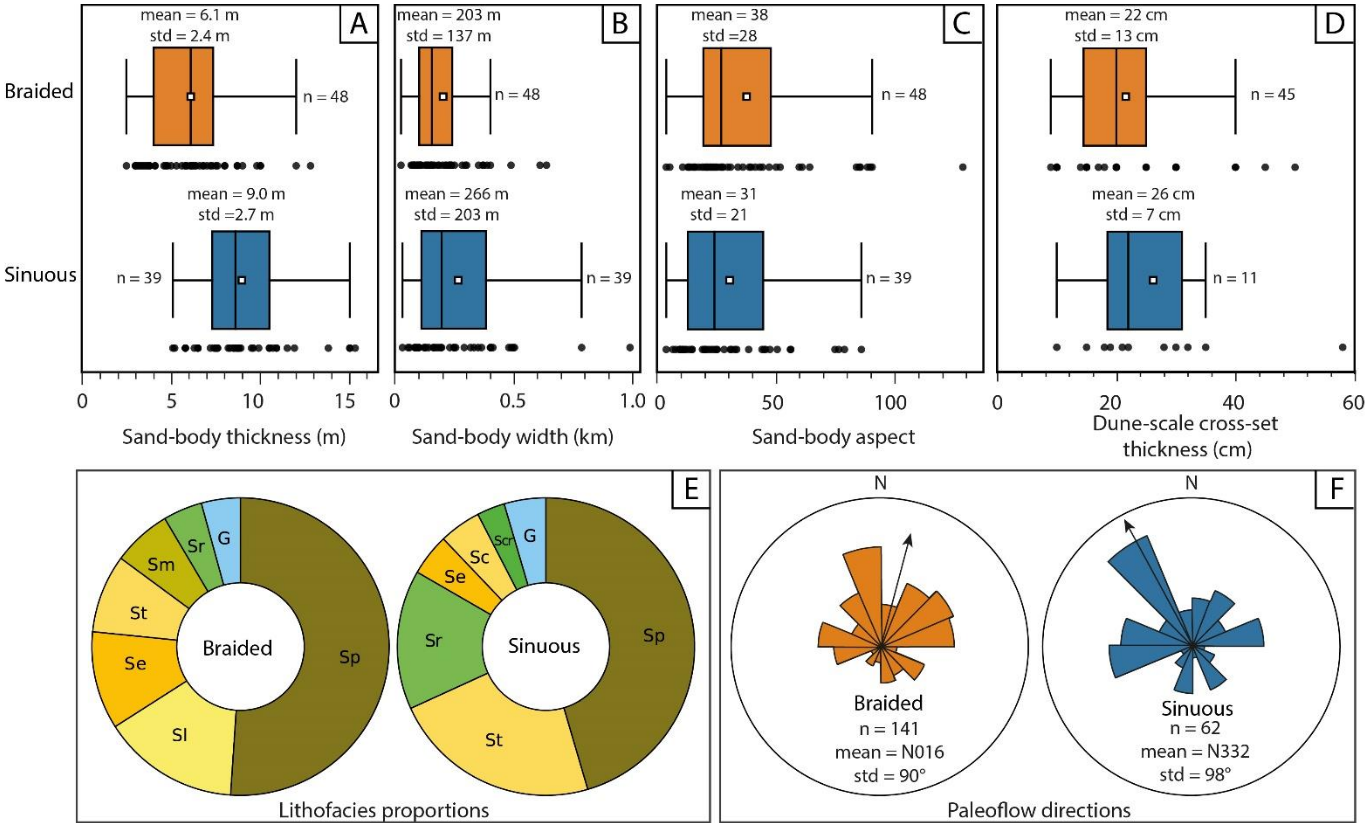

Figure 7. (A) Thicknesses, (B) widths, and (C) aspects of braided and sinuous channel sandstone bodies. (D) Thicknesses of dune–scale cross–sets. (E) Relative abundance of different lithofacies within braided and sinuous sandstone bodies (abbreviations are listed in Table 1). (F) Rose diagrams of palaeoflow directions. Note the significantly thinner and insignificantly narrower braided deposits than sinuous counterparts, the similarity and difference between relative lithofacies abundance, and the similarity and difference between paleoflow directions.

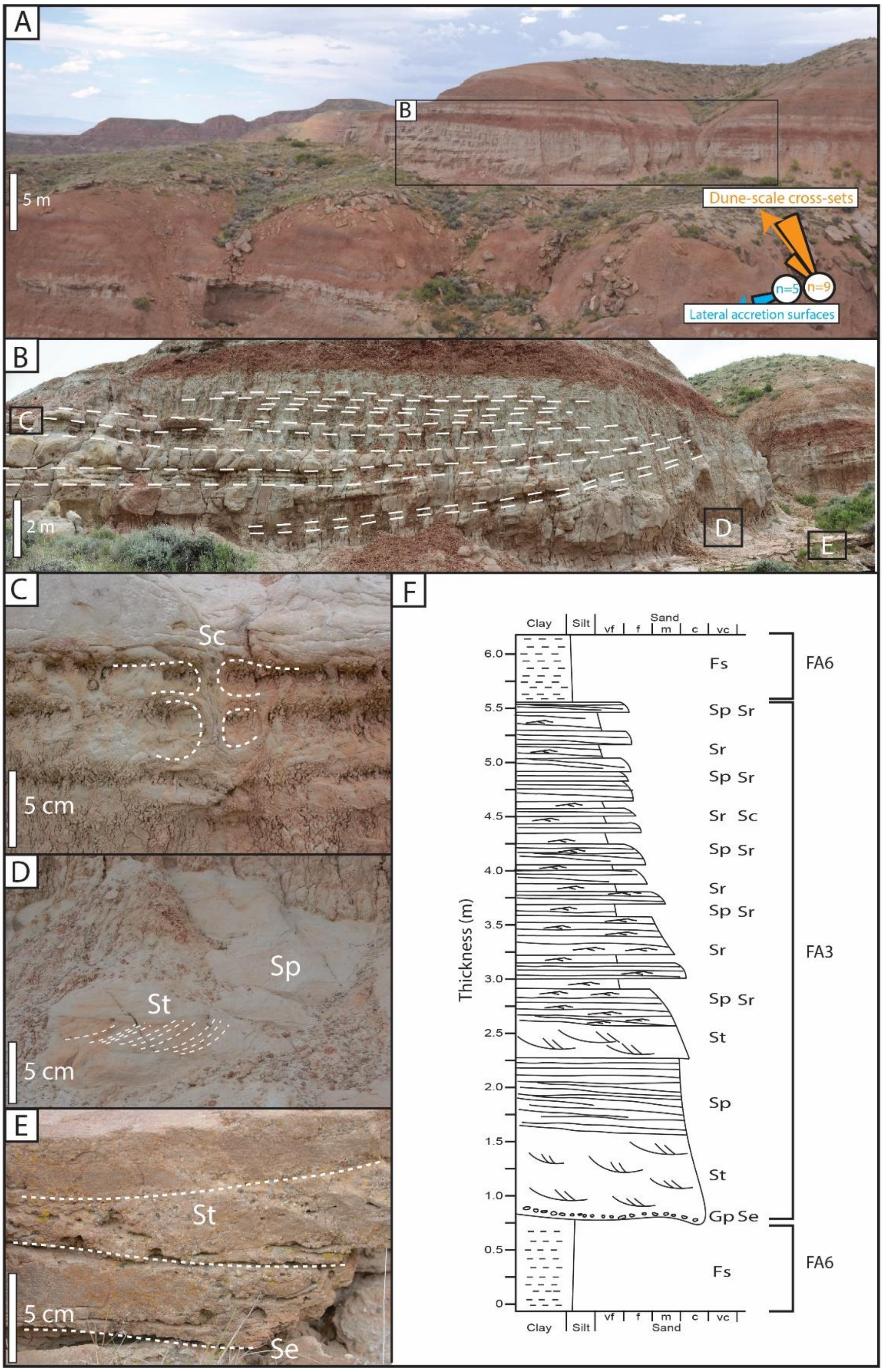

Figure 8. Facies Association 4: sinuous channel sandstone deposits. (A) Overview photo showing the juxtaposition between FA4 and surrounding strata. (B) Enlarged view of the FA4 deposits, where lateral accretion deposits are distinct. (C) Convolute sandstone with clear water escape structures. (D) Trough and planar cross-bedding with a dominant flow direction of 10°. (E) Channel-floor deposits at the base of FA4. (F) Composite sedimentary log illustrating the vertical succession of lithofacies in FA4. For legend, see Figure 3.

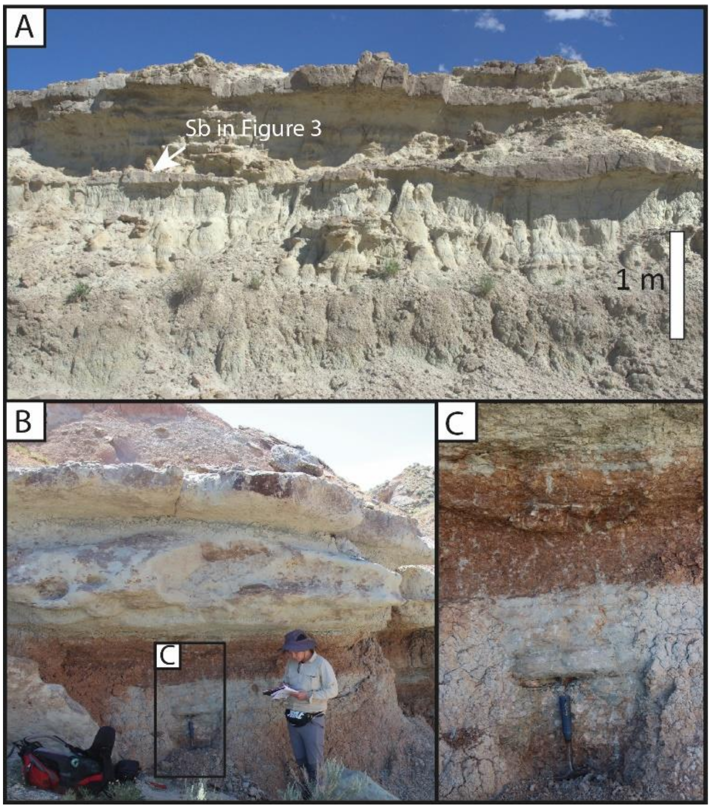

Figure 9. Facies Associations 5 and 6. (A) Heterolithic, weakly pedogenic deposit interpreted as crevasse splay deposit. (B-C) Strongly pedogenically-modified deposits interpreted as overbank deposits. The person for scale is ~1.8 m, and the hammer for scale is ~25 cm long.

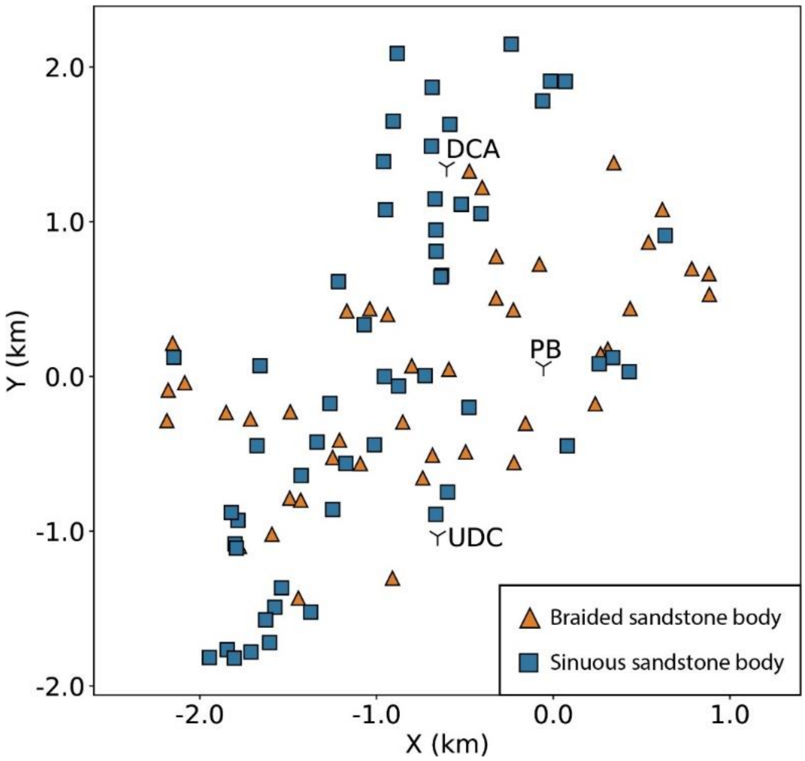

Figure 10. Projection of sandstone bodies from 3D space to 2D XY horizontal plane. X and Y coordinates are converted from global UTM coordinates (zone 12N) to local ones, with an applied offset of (673000 m, 49242600 m). Locations of DCA, PB, and UDC sections can be compared with those in Figure 2.

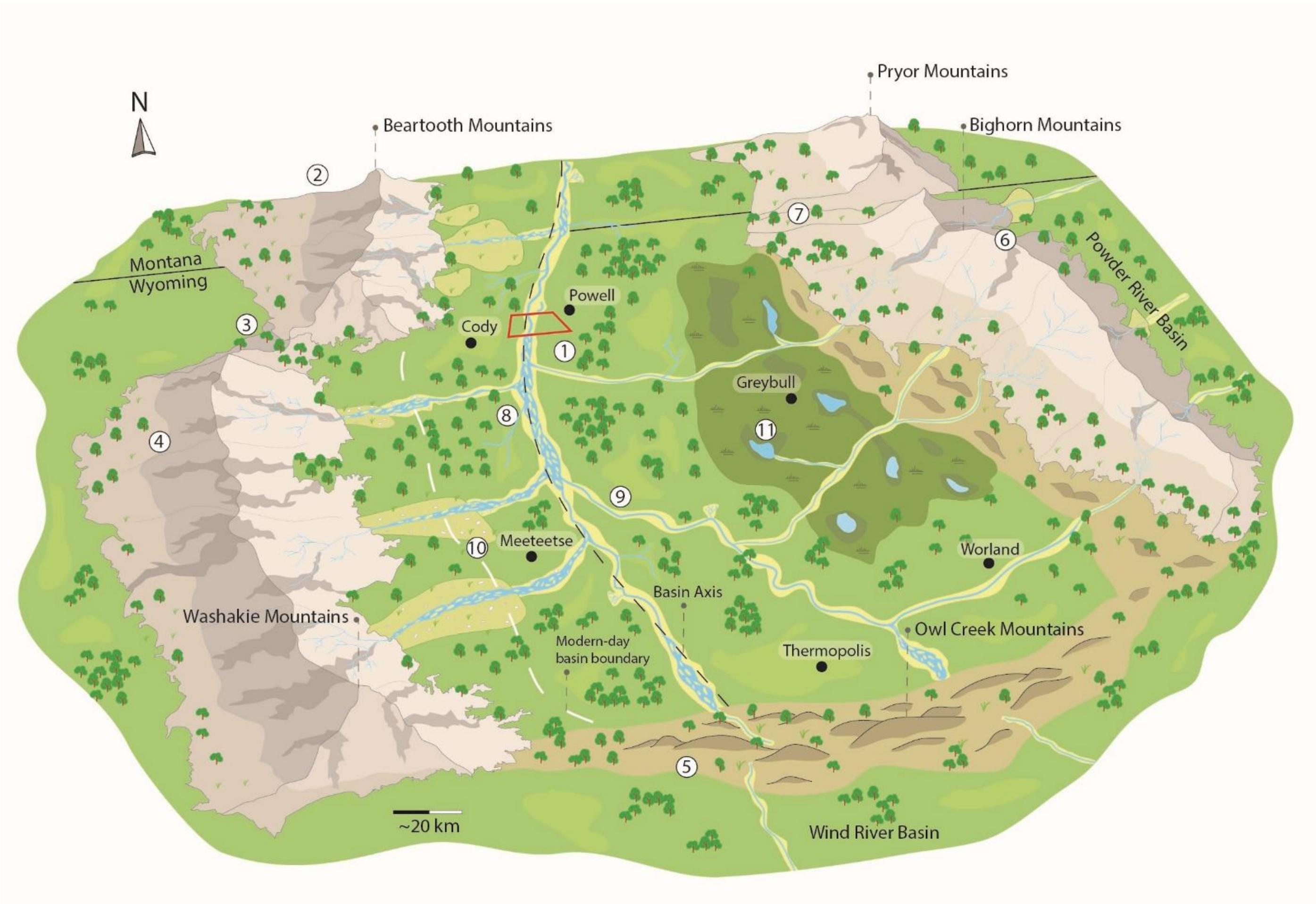

Figure 11. Schematized palaeogeographic model of the Bighorn Basin during the early Eocene. Annotations for elements marked with numbers in the figure are as follows: (1) The McCullough Peaks study area. (2) The Beartooth Mountains with a very steep eastern flank (Bown, 1980) and several ephemeral coarse-grained alluvial fans and braid-plain deposits (DeCelles *et al.*, 1991). (3) The space between the Washakie mountains and the Beartooth during Eocene is uncertain in the literature due to the covering of the Absaroka Mountains. (4) Washakie Mountains are not present today (Kraus, 1985), because they are covered by volcanic Absoraka Mountains (Sundell, 1990). (5) The Owl Creek Hills were relatively gentle in Eocene (Wing & Bown, 1985). (6) Unlike the present day, the Bighorn mountains were much smaller and not fully formed in the Eocene (Yonkee & Weil, 2015). The small fine-grained sediment input from the Bighorn Mountains into the Bighorn Basin is due to the large distance and gentle topography from the mountains to the axis. (7) Pryor Gap could be an exit for the rivers during the Eocene (Blackstone, 1940). However, there are no constraints on when it opened. (8) Braided channel belt with downstream accretion deposits. (9) Sinuous channel belt with crevasse splay, local/regional avulsion, and point bars. (10) Fanglomerates on the alluvial fan (Kraus, 1983, 1984), indicating a near-source system. (11) Swampy and lacustrine environment in front of the Bighorn Mountains (Wing & Bown, 1985; Davies-Vollum & Wing, 1998).

Table 1. Description and interpretation of lithofacies in the McCullough Peaks stratigraphy.

Lithofacies code	Description	Interpretation
Clast-supported conglomerate (**G**)	Poorly sorted, granule to small pebble conglomerate, with medium-grained angular sandstones as the matrix. The conglomerate fills erosional scours and can also be organized in 20 to 60 cm thick beds at the base of sandstone bodies.	Intrabasinal clasts of floodplain mudstones or granules deposited by subcritical to supercritical traction flow.
Massive sandstone (**Sm**)	Fine to medium-grained sandstone, well-sorted, no apparent sedimentary structures, a few decimeters in thickness.	High rate of deposition, probably formed during high-discharge periods.
Trough cross-stratified sandstone (**St**)	Fine- to coarse-grained, well-rounded sandstone forming up to 50 cm thick cross-stratified beds. Preserved set thickness varying between 5 and 30 cm, often decreasing upward in the bed. Sets in the basal part of a sandstone body are often poorly sorted and may contain granules; sets in the top of a bed are better sorted. Claystone chips are common. Bed boundaries are slightly inclined (up to 2 degrees).	Subcritical flow, normal deposition rates, bedload deposition, dune migration.
Planar/Tabular cross-stratified sandstone (**Sp**)	Fine- to medium-grained, well-rounded, and moderate- to well-sorted lithic sandstone forming up to 30 cm thick cross-stratified beds. Preserved set thickness varying between 5 and 20 cm, often decreasing upward in the bed. Bed boundaries are slightly inclined.	Supercritical flow, normal deposition rates, bedload deposition, plane bed formation.
Ripple cross-laminated sandstone (**Sr**)	Very fine to fine-grained sandstone, well-sorted, ripple lamination with a set thickness of 2-5 cm.	Ripple migration under the low-flow regime.
Climbing-ripple cross-laminated sandstone (**Scr**)	Fine-grained sandstone, moderately to well sorted, asymmetrical cross lamination with climbing set boundaries, with a bed set thickness of 2-5 cm.	Subcritical flow, faster deposition than ripple migration due to abundant sediments in suspension.
Low-angle (<15°) cross-bedded sandstone (**Sl**)	Fine to medium-grained sandstones, well-rounded, moderately to well-sorted, bed thickness of 0.1-1 m. Low-angle stratification with a long wavelength and low angle.	Deposition under upper-flow-regime conditions during high-stage flooding events in nearby channels.
Sandstone with erosional scour and fill (**Se**)	Fine to medium-grained poorly sorted sandstones, with sand-supported nodules (0.5-2 cm in diameter) filling the scours, thickness of 0.2-1 m.	Supercritical flow causing the scour, high deposition rates, with nodules as lag deposits
Bioturbated sandstone (**Sb**)	Fine- to medium-grained sandstone, moderately to poorly sorted, with vertical and horizontal burrows and trace fossils.	Trace fossils formed by insets, dwelling, resting, crawling
Convoluted sandstone (**Sc**)	Fine- to medium-grained, well-rounded, moderately to well-sorted lithic sandstone. Preserved set thickness varying between 5 and 20 cm, often decreasing upward in the bed. Overturned-fold-shaped structures that modified or destroyed primary sedimentary structures, with a size of 20-60 cm.	Water escape structures formed in rapidly deposited, poorly sorted sands
Mudstones and siltstones (**Fs**)	Clay to siltstone, with laminated or blocky structures, various matrix colours, frequently seen slickensides and nodules.	Soil formation with chemical precipitation developed on former overbank fines.
Laminated siltstones (**Fl**)	Well sorted siltstones with ripple laminations.	Settling from suspension and forming silty plug in the abandoned channel.

Supplementary figures

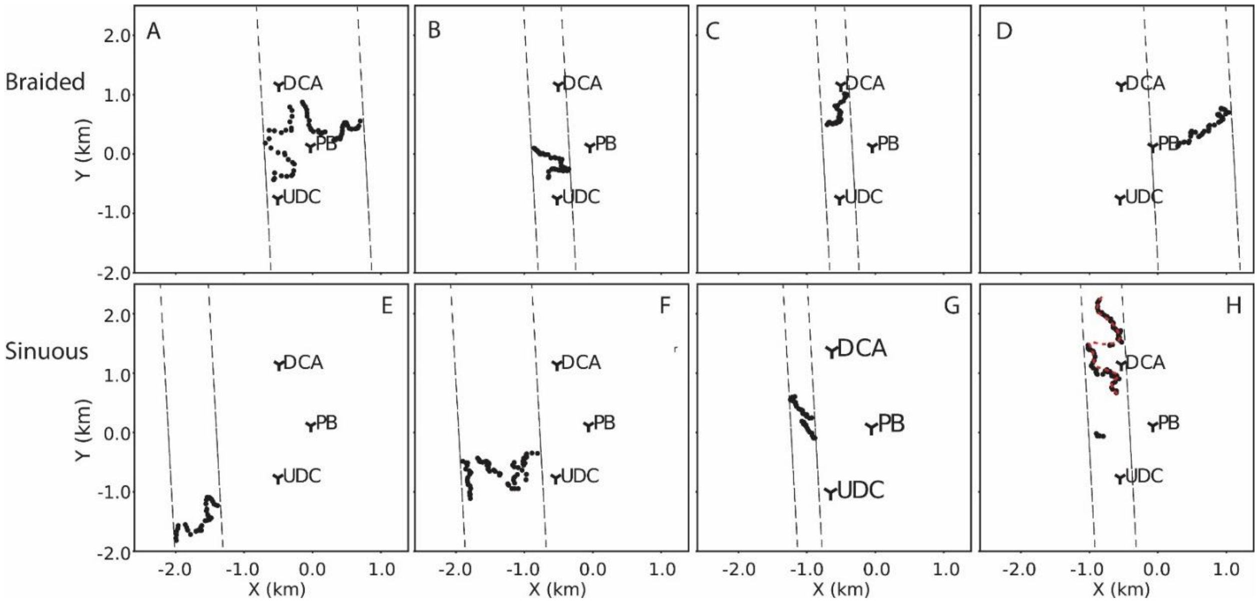

Figure S1. (A-D) Four examples showing how widths of braided channel sandstone bodies are measured. (E-H) Four examples showing how widths of sinuous channel sandstone bodies are measured. The black dots indicate the presence of the sandstone body at the outcrop surface, and two dashed boundary lines are along the average paleoflow direction (4°N). A sinuosity index is calculated in subfigure H, indicated by the red dot line. Locations of DCA, PB, and UDC sections can be found in Figure 2 for comparison.

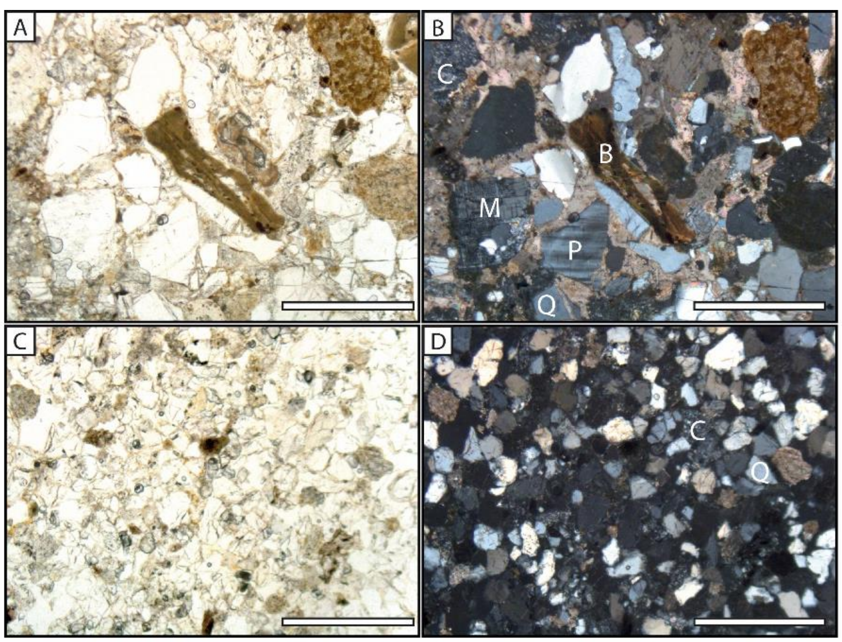

Figure S2. Petrographic characteristics of braided and sinuous deposits. (A, B) Thin sections of braided channel deposits under plane- and orthogonally-polarized light. (C, D) Thin sections of sinuous channel deposits under plane- and orthogonally-polarized light. B = biotite; C = chert; M = microline; P = plagioclase; Q = quartz. White bar for scale is 500 µm.

Supplementary tables

Table S1. Presence of facies in each facies association

Facies associations	Containing facies
FA1 (small-scale cut-and-fill channel sandstone deposits)	St, Sp, Sr
FA2 (large-scale massive trunk-shaped channel sandstone deposits)	G, St, Sp, Sr, Sc
FA3 (braided channel sandstone deposits)	G, Se, St, Sp, Sr, Sc, Sl
FA4 (sinuous channel sandstone deposits)	G, Se, St, Sp, Sr, Sc, Fl
FA5 (crevasse splay deposits)	St, Sl, Sr, Sb
FA6 (overbank palaeosol deposits)	Fs